National Library of Canada

Bibliothèque nationale du Canada

Acquisitions and Bibliographic Services Branch

Direction des acquisitions et des services bibliographiques

395 Wellington Street
Ottawa, Ontario
K1A 0N4

395, rue Wellington
Ottawa (Ontario)
K1A 0N4

Your file Votre référence

Our file Notre référence

NOTICE

The quality of this microform is heavily dependent upon the quality of the original thesis submitted for microfilming. Every effort has been made to ensure the highest quality of reproduction possible.

If pages are missing, contact the university which granted the degree.

Some pages may have indistinct print especially if the original pages were typed with a poor typewriter ribbon or if the university sent us an inferior photocopy.

Reproduction in full or in part of this microform is governed by the Canadian Copyright Act, R.S.C. 1970, c. C-30, and subsequent amendments.

AVIS

La qualité de cette microforme dépend grandement de la qualité de la thèse soumise au microfilmage. Nous avons tout fait pour assurer une qualité supérieure de reproduction.

S'il manque des pages, veuillez communiquer avec l'université qui a conféré le grade.

La qualité d'impression de certaines pages peut laisser à désirer, surtout si les pages originales ont été dactylographiées à l'aide d'un ruban usé ou si l'université nous a fait parvenir une photocopie de qualité inférieure.

La reproduction, même partielle, de cette microforme est soumise à la Loi canadienne sur le droit d'auteur, SRC 1970, c. C-30, et ses amendements subséquents.

Canada

UNIVERSITY OF ALBERTA

PHOSPHORUS-DOPED GLASS WAVEGUIDES ON SILICON SUBSTRATES

BY

RAJASHREE NARENDRA

A thesis submitted to the Faculty of Graduate Studies and Research in partial fulfillment of the requirements for the degree of **MASTER OF SCIENCE.**

DEPARTMENT OF ELECTRICAL ENGINEERING

EDMONTON, ALBERTA
Fall 1992

National Library of Canada
Bibliothèque nationale du Canada

Canadian Theses Service
Service des thèses canadiennes

Ottawa, Canada
K1A 0N4

The author has granted an irrevocable non-exclusive licence allowing the National Library of Canada to reproduce, loan, distribute or sell copies of his/her thesis by any means and in any form or format, making this thesis available to interested persons.

L'auteur a accordé une licence irrévocable et non exclusive permettant à la Bibliothèque nationale du Canada de reproduire, prêter, distribuer ou vendre des copies de sa thèse de quelque manière et sous quelque forme que ce soit pour mettre des exemplaires de cette thèse à la disposition des personnes intéressées.

The author retains ownership of the copyright in his/her thesis. Neither the thesis nor substantial extracts from it may be printed or otherwise reproduced without his/her permission.

L'auteur conserve la propriété du droit d'auteur qui protège sa thèse. Ni la thèse ni des extraits substantiels de celle-ci ne doivent être imprimés ou autrement reproduits sans son autorisation.

ISBN 0-315-77292-1

Canadä

UNIVERSITY OF ALBERTA

RELEASE FORM

NAME OF AUTHOR: **RAJASHREE NARENDRA**

TITLE OF THESIS: **PHOSPHORUS-DOPED GLASS WAVEGUIDES ON SILICON SUBSTRATES**

DEGREE: **MASTER OF SCIENCE**

YEAR THIS DEGREE GRANTED: **1992**

Permission is hereby granted to the University of Alberta Library to reproduce single copies of this thesis and to lend or sell such copies for private, scholarly or scientific research purposes only.

The author reserves all other publication and other rights in association with the copyright in the thesis, and except as herein before provided neither the thesis nor any substantial portion thereof may be printed or otherwise reproduced in any material form whatever without the author's prior written permission.

Rajashree Narendra

Rajashree Narendra

525, 20th Main road
4th T Block, Jayanagar
Bangalore - 560011
Karnataka, India

July 8, 1992
Date

UNIVERSITY OF ALBERTA

FACULTY OF GRADUATE STUDIES AND RESEARCH

The undersigned certify that they have read, and recommend to the Faculty of Graduate Studies and Research for acceptance, a thesis entitled **PHOSPHORUS-DOPED GLASS WAVEGUIDES ON SILICON SUBSTRATES** submitted by **RAJASHREE NARENDRA** in partial fulfillment of the requirements for the degree of **MASTER OF SCIENCE.**

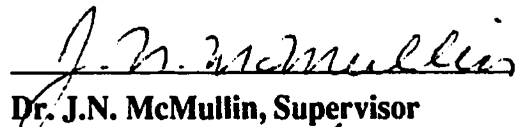

Dr. J.N. McMullin, Supervisor

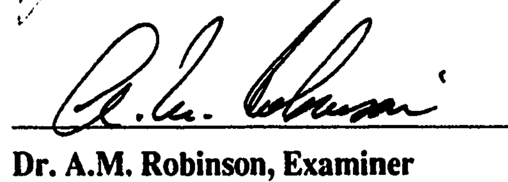

Dr. A.M. Robinson, Examiner

Dr. W. Allegretto, External Examiner

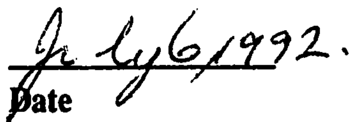

Date

To my dearest sister and family,
(Viju, Anand and Deepti)

I dedicate this thesis in your memory.
I will miss you all a lot.

ABSTRACT

Phosphorus-doped glass waveguides have been formed on silicon substrates by chemical vapor deposition (CVD). The waveguides are made up of three layers; namely, silicon dioxide as the buffer layer, phosphorus-doped glass as the core and silicon dioxide as the cladding layer. The two types of waveguides discussed are the slab and channel waveguides. Single-mode, phosphorus-doped glass slab waveguides with step index profile have been fabricated. The slab waveguides provide a simple approach to test the design and fabrication procedure, and have potential use in semi-free-space optical interconnects. The estimated thickness of the core, buffer and cladding are 1.16 μm, 4.5 μm and 3.0 μm respectively. The phosphorus-doped glass slab waveguides exhibited a low loss of 0.05 dB/cm at 0.6328 μm wavelength.

Also, single-mode, phosphorus-doped glass channel waveguides have been fabricated in silicon V-grooves. These waveguides have been coined as "Nabla" waveguides because their geometry resembles the nabla symbol "∇". A novel fabrication technique is reported, which is reproducible and involves few steps. These low-loss waveguides have the potential for doped active devices such as lasers and optical amplifiers. The width and depth of the core to support single-mode propagation is 1.88 μm and 1.33 μm. The estimated thickness of the buffer and cladding are 4.5 μm and 3 μm respectively. The phosphorus-doped glass channel waveguides exhibited a low loss of 0.1 dB/cm at the Helium-Neon wavelength of 0.6328 μm. The mode field diameter of the phosphorus-doped glass channel waveguide is 7.4 μm at 0.6328 μm wavelength, measured by imaging the near-field mode profile. The measured mode profiles are compared with the theoretical predictions.

ACKNOWLEDGEMENTS

I thank my husband, **Narendra Viswanath** for his co-operation and support throughout my studies.

It gives me great pleasure to express my deep gratitude to **Dr. J.N. McMullin,** my supervisor, for his strong overwhelming support, advice, encouragement, rewarding suggestions and discussions throughout this project. **Dr. McMullin** has been the source of inspiration for the successful completion of this thesis.

I thank the **Telecommunication Research Laboratories** for the scholarship and the measurement facility. I owe the successful completion of this project to **Alberta Microelectronic Center**, for their support and process facility. I thank the **Department of Electrical Engineering** for the Teaching Assistance and other facilities.

I also owe a great deal of thanks to number of individuals for the help they have extended:

Dr. Ian McDonald, TR labs, for his active participation in this project.

Graham McKinnon, AMC, for his active participation, support and helpful discussions throughout this project and also for the help with the mask design.

Yan Loke, AMC, for his co-operation and immense help with the photolithography process, annealing and EDP etching.

Glen Fitzpatrick, AMC, for his co-operation and immense help with the CVD deposition, sputtering and SEM pictures.

Alan Mitchell, AMC, for the deposition of metal films and reflectivity measurements.

Tran-Tran, AMC, for his help with the dicing machine.

Yeubin Ning, AMC, for his help with the EDP etching.

Harold Peacock, AMC, for his help with the mask design.

Barry Arnold, Dept. of Electrical Engineering, for advise on polishing and process details.

Dr. Barry Keyworth, TR labs, for his immense help with the measurement set-up and mode field measurements.

Dave Clegg, TR labs, for his help with the equipment set-up.

Andre Delage, NRC, for theoretical calculations of the mode profile.

Dr. Sujeet Chaudhari and W. Huang, University of Waterloo, for theoretical calculations of the mode profile.

Senthil Kumar, my colleague, for helpful discussions.

Finally, I thank my family and friends for all the co-operation and help they have extended.

TABLE OF CONTENTS

CHAPTER	PAGE
1. INTRODUCTION	1
2. REVIEW OF INTEGRATED OPTICAL WAVEGUIDES	5
2.1 Basic principles	5
2.2 General desirable properties	5
2.3 Waveguide classification	8
(a) Slab waveguides	8
(b) Channel waveguides	11
3. SLAB WAVEGUIDES	14
3.1 Design	14
3.2 Fabrication	15
3.3 Loss measurement set-up	18
4. NABLA WAVEGUIDES	23
4.1 Design	23
4.2 Fabrication	23
(a) General plan	23
(b) Fabrication Details	24
(i) Substrate preperation	24
(ii) Photolithography	27
(iii) Anisotropic etching	27
(iv) Deposition of buffer and core layers	28
(v) Annealing and etching	30
(vi) Deposition of the cladding layer	36
(vii) Deposition of the metal film for taps	36
4.3 Loss measurement	37
4.4 Near-field intensity measurement	37

5. CONCLUSIONS 48

BIBLIOGRAPHY 50

APPENDIX 1 55

A.1.1 Design of single-mode slab waveguide 55

A.1.2 Suprem III diffusion process modeling 56

APPENDIX 2 58

A.2.1 Design of single-mode channel waveguide 58

APPENDIX 3 61

A.3.1 Photolithography recipe 61

A.3.2 Anisotropic etchant for silicon 62

A.3.3 Low-pressure chemical vapor deposition 63

A.3.4 Deposition of various metal films 66

APPENDIX 4 73

LIST OF TABLES

TABLE		PAGE
A.4.1	Loss data of annealed phosphorus-doped glass slab waveguide 1.	73
A.4.2	Loss data of annealed phosphorus-doped glass slab waveguide 2.	74
A.4.3	Loss data of unannealed phosphorus-doped glass slab waveguide 1.	75
A.4.4	Loss data of unannealed phosphorus-doped glass slab waveguide 2.	76
A.4.5	Loss data of phosphorus-doped glass channel waveguide 1.	77
A.4.6	Loss data of phosphorus-doped glass channel waveguide 2.	78
A.4.7	Horizontal scan data of the output mode profile	79
A.4.8	Vertical scan data of the output mode profile	81

LIST OF FIGURES

FIGURE		PAGE
2.1	Different types of possible modes when $n_f > n_s, n_c$	6
2.2	Slab waveguide	9
2.3	Different types of refractive index profiles	9
2.4	Different types of channel waveguides	12
3.1	Refractive index (n) of the doped SiO_2 vs. the phosphine flow rate (cc/min)	16
3.2	Phosphorus-doped glass slab waveguide	17
3.3	Set-up for measuring the slab waveguide scattering losses	19
3.4	Attenuation plots of annealed phosphorus-doped glass slab waveguides	21
3.5	Attenuation plots of unannealed phosphorus-doped glass slab waveguides	22
4.1 (a)	Silicon V-groove with 4.5 µm silicon dioxide, 1 µm phosphosilicate glass and 8.0 µm silicon dioxide	25
4.1 (b)	Under-etching of the oxide due to the crack	25
4.2	Fabrication of the phosphorus-doped glass nabla waveguides	26
4.3	Wafer processing technique	29
4.4 (a-f)	Scanning electron micrographs of the etch-back technique	32
4.5 (a)	Silicon V-groove with 4.5 µm silicon dioxide, 2.5 µm phosphosilicate glass and 3.0 µm silicon dioxide	35
4.5 (b)	Silicon V-groove with 4.5 µm silicon dioxide, 2.5 µm phosphosilicate glass and 4.0 µm spin-on-glass	35
4.6	Set-up for measuring the channel waveguide scattering losses	38
4.7	Attenuation plots of phosphorus-doped glass channel waveguides	39
4.8	Schematic of the near-field intensity measurement	40
4.9	Image and the contour plot of the output mode of the single-mode channel waveguide	43

4.10 Output mode linear and 3-D profile 44

4.11 Horizontal and vertical scan of the output mode profile 45

4.12 Theoretical mode profiles at 0.6328 μm and 1.3 μm 46

4.13 Beam profile in waveguide after 1.6 mm of propagation of an optical input beam. 47

A.1.1 Step index profile 55

A.1.2 Diffusion of 10 wt. % phosphorus in silicon dioxide using Suprem III process modelling 57

A.2.1 Geometry of the triangular core and cylindrical fiber 58

A.2.2 Minimum SiO_2 buffer layer thickness required to reduce the leakage loss of waveguides on SiO_2 /Si 60

A.3.1 Low-pressure chemical vapor deposition chamber 64

A.3.2 Characterization of the surface properties of the metal films with oxide 69

LIST OF SYMBOLS

Å - Angstrom

Al - Aluminum

Au - Gold

A - Area

a - Asymmetry measure

cc/min - Cubic centimeter per minute

cm - Centimeter

°C - Degree centigrade

2-D - Two dimensional

3-D - Three dimensional

d - Depth

dB - Decibels

GaAs - Gallium arsenide

GaAlAs - Gallium aluminum arsenide

Hz - Hertz

He - Helium

λ – Lambda

$LiNbO_3$ - Lithium niobate

$LiTaO_3$ - Lithium tantalate

log - Logarithm

μm - Micron

min - Minute

ml - Milliliter

mm - Millimeter

∇ – Nabla

N_2 - Nitrogen

n - Refractive index

n_s - Refractive index of the substrate

n_f - Refractive index of the guiding film

n_c - Refractive index of the cladding

Nb_2O_5 - Niobium oxide

Ne - Neon

nm - Nanometer

psi - Pounds per square inch

PH_3 - Phosphine

rpm - Revolutions per minute

III-V semiconductors - GaAs & GaAlAs

sccm - Standard cubic centimeter per minute

sec - Seconds

Si - silicon

SiC - Silicon carbide

SiH_4- Silane

Si_3N_4 - Silicon nitride

SiO_2 - silicon dioxide

Ta_2O_5 - Tantallum oxide

V - Normalized frequency

W - Width

wt. % - Weight percent

ZnO - Zinc oxide

LIST OF ABBREVIATIONS

AMC - Alberta Microelectronics Center
BOE - Buffer oxide etch
CVD - Chemical vapor deposition
DC - Direct current
EDP - Ethylene diamine pyracatechol
FWHM - Full width half maximum
HIPOX - High pressure steam oxide
HMDS - Hexamethylene disilazane
LPCVD - Low-pressure chemical vapor deposition
LTO - Low-temperature oxidation
OEIC - Optoelectronic integrated circuits
MFD - Mode field diameter
NA - Numerical aperture
PR - Photoresist
PMMA - Polymethyl methacryalate
PSG - Phosphosilicate glass
PXL - Pixel
RF - Radio frequency
SEM - Scanning electron microscope
SOG - Spin-on-glass
SM - Single-mode
TEOS - Tetraetyl orthosilicate
TE - Transverse electric
TM - Transverse magnetic
TV - Television
UV - Ultraviolet
VCR - Video cassette player
VLSI - Very large scale integration
WG - Waveguide
WMUX - Wavelength multiplexer / demultiplexer

1. INTRODUCTION

Integrated optics refers to the application of thin film technology to the fabrication of small-scale optical systems. The basic idea behind this technology involves the trapping of light by means of total internal reflection within the confines of an optical waveguide. The light propagating within the waveguide can be manipulated by components formed in or on that same waveguide structure. Integrated optics provides compact, high-speed, low drive power, mass producible optical components for communications and signal processing applications. In 1969, Miller [1], recognizing the inconvenience of placement and alignment of all optical components on light benches and the limits imposed by that inconvenience, suggested the concept of integrated optics. Since then, the field of integrated optics has attempted to compress the large light bench of assorted optical components onto single substrates.

Integrated optics is the optical counterpart of integrated electronics. This implies that integrated optical systems control signals in the form of light beams within the miniaturized components fabricated on a single substrate. At the board or wafer level, simple techniques for fabricating optical channels within the electronic system are needed. There are two approaches for integrating a higher level of optics and electronics. The first approach is the optoelectronic integrated circuit (OEIC), where all the functions take place on a monolithically grown and processed wafer. The second approach is hybrid, where different devices are combined on a common substrate using surface mounting techniques and interconnects are made with optical waveguides. In principle, hybrid technology can accommodate a wide range of complexity by allowing the best combination of devices to realize the optimum system performance. Eventually hybrid technology will provide the optical bench, the controlled environment and the interface to the outside world for increasingly complex OEICs.

Many signal processing functions needed for optical communications and switching networks have been effectively implemented in waveguide systems where optoelectronic integrated circuits serve as intelligent control points capable of recognizing and processing the optical signals as required. Integrated optic radio frequency spectrum analyzers, analog-to-digital converters, convolvers and correlators, and optical switches like the directional coupler, branching waveguide and total internal reflection switch are a few of the available optical integrated circuits used in optical communication and signal processing applications [2]. There has been considerable interest in the application of integrated optics to sensors. With an

increase in integration, optical integrated circuits become more functional but difficult to fabricate.

The evolution of integrated optics technology relies on innovative design and fabrication techniques using advanced material technology. The five advanced materials that have attracted attention as bases for integrated optical systems are gallium arsenide-gallium aluminum arsenide (GaAs-GaAlAs), lithium niobate ($LiNbO_3$), indium phosphide (InP), glass and silicon (Si). The selection of a suitable substrate material is important when one has to implement some function in integrated optoelectronics. By listing only the physical characteristics required for designing integrated optical circuits, one concludes that lithium niobate is certainly the best compromise among all the potential materials since it associates good optical quality, low-loss waveguides and good physical properties including high electrooptic and electromechanical coupling coefficients and low surface-acoustic-wave losses. However a substrate material is not only interesting because of its physical characteristics. Fully developed technological equipment and processes are needed to ensure that the components exhibit good reproducibility and performance. From this point of view semiconductors are the most favorable. Silicon and the III-V semiconductors also offer the possibility of the integration of high-speed electronic components with the optical components.

Silicon as a substrate offers a number of unique advantages:

(1) **Good thermal properties**: Free to solder the devices to the guides at temperatures ~400^0C. Also can be annealed at high temperatures to achieve optimal properties.

(2) **Good electrical properties**: Silicon can be an insulator or conductor depending on the processing.

(3) **Optical bench**: The <111> planes can be used to align optical components. Silicon can be micro-machined to hold fibers, lenses, devices and lids in excellent registration. The high thermal conductivity of silicon makes it a good substrate for bonding active components to form hybrid devices.

(4) **Good mechanical stability**: Can align optical components with great stability.

(5) **Compatibility** with integrated circuit manufacturing.

Silicon is an attractive material because of its dominance and maturity in the microelectronics industry. It continues to attract interest, in spite of its indirect bandgap and the absence of an electrooptic effect, for the simple reason that silicon processing technology is so advanced and the electronics industry is so mature. Silicon substrates offer ease of connection with various surrounding elements

including laser diodes, photodetectors and optical fibers. Silicon is not only an excellent substrate for passive optical waveguides, but also for a hybrid technology that potentially incorporates all optoelectronic components on the same wafer. Silicon has the potential of producing low cost optoelectronic packaging as well as integrated optical circuits. Silicon will be useful as a source of complex passive integrated optical circuits such as fanouts, star couplers and multiple channel multiplexers. It also has the potential to be a practical substrate for the fabrication of narrow-line lasers and many other hybrid optoelectronic devices [3].

Silicon provides an excellent surface for the formation of a variety of waveguide structures, and its pattern processing technology is well established. Chemical vapor deposition (CVD) is widely used to deposit thin films in semiconductor processing. Chemical-vapor-deposited glass is used as a optical waveguide material. The properties of glass are altered by the addition of dopants. Phosphorus is one of the most common and least expensive doping elements. The refractive index of glass increases linearly with the increase in phosphorus doping concentration [4]. CVD phosphorus-doped glass waveguides are used to fabricate four-port polarization splitters [3], multichannel star couplers [5], four-channel Mach-Zehnder multiplexers/demultiplexers [6], wavelength multiplexers/demultiplexers (WMUX) [7], adiabatic tapers [8], adiabatic polarization splitters [9], geodesic optical waveguide lenses [10], and optical ring resonators [11].

Anisotropic etching of silicon has become an important technology in silicon semiconductor processing. In silicon micro-machining the oxide is used as a mask during the chemical etching, the anisotropic etchants attack the silicon underlying openings in the oxide layer excavating three dimensional pits in the wafer. A rectangular opening oriented along the <110> directions of a <100> wafer yields a V-shaped groove with {111} side walls. Controlled etching of silicon, which is required to fabricate devices with a predictable geometry depends on an accurately oriented, defect-free substrate, well-defined and aligned pattern geometry and rigorously clean etching conditions. Anisotropic etching of single-crystal silicon resulting from the differential etch rate of its crystallographic planes has been used to fabricate a variety of active and passive, three-dimensional device structures which include jet nozzles, motors, multisocket electrical connectors, multichannel arrays for fiber alignment and optical channel waveguides, miniature circuit boards and optical benches [12-14].

Low-loss, single-mode silica fibers are commonly used in almost all telecommunications applications. Although there have been rapid advances made during the last few years in the field of integrated optics, the problem of providing

efficient and convenient coupling between an integrated single-mode waveguide and silica fiber still remains largely unsolved. Recently, however, silicon V-grooves have been used as optical fiber alignment grooves [15]. Therefore the technique of fabricating integrated silica waveguides in silicon V-grooves lends itself to good coupling efficiency. Efficient coupling can be achieved if the optical modes of the fiber and the channel waveguide are similar.

This research involves the fabrication of slab and channel phosphorus-doped glass waveguides on silicon substrates using the CVD process. The waveguides have a step index profile and have been designed to obtain single-mode propagation. The slab waveguides provide a simple approach to test the design and fabrication procedure. The slab waveguides have potential use in semi-free-space optical interconnects [16]. We have coined the name "Nabla waveguides" for phosphorus-doped glass channel waveguides formed in silicon V-grooves because their geometry resembles the nabla symbol "∇". These low-loss waveguides can be designed to be compatible with an optical fiber. It may be possible to obtain out-of-plane coupling from these waveguides. The channel waveguides have the potential for doped glass active devices such as optical amplifiers and lasers.

Integrated optical waveguides are reviewed in Chapter 2. The design, fabrication, and loss measurements of the phosphorus-doped glass slab waveguide are described in Chapter 3. Chapter 4 describes design, fabrication, loss and mode profile measurements of V-groove waveguides. The results and recommendations are discussed in Chapter 5. The Appendices describe in detail the design of the slab and channel waveguides, recipes of photolithography, etching and CVD processes, and characterization of metal films.

2. REVIEW OF INTEGRATED OPTICAL WAVEGUIDES

2.1 BASIC PRINCIPLES:

The most basic element in integrated optics is the optical waveguide. Generally speaking, an optical waveguide consists of a high index core regions surrounded by lower index cladding regions. The thin film optical waveguide consists of three different layers; namely, the substrate or the buffer layer, the guiding layer (core) and the over layer (cladding) as shown in Figure 2.1. The light is trapped in the thin film by total internal reflection and propagates within the layer as long as the condition $n_f > n_s, n_c$ is satisfied, where n_s, n_f, and n_c are the indices of refraction of the substrate, guiding film and cladding layer respectively.

Mathematically, the problem of wave propagation in a waveguide involves solving Maxwell's equations in the various layers and joining the solutions by matching the boundary conditions at the interfaces between layers. These solutions indicate two types of modes of propagation, bound modes and radiation modes. In a bound mode, the energy is confined within the waveguide structure (Figure 2.1a). In a radiation mode, the energy radiates into either the substrate (Figure 2.1b) or the substrate and cladding (Figure 2.1c).

We are interested primarily in the bound modes of the waveguide. The waveguide modes depend upon the thickness of the waveguide core and the values of the refractive indices of the core and cladding layers. Each mode has its own transverse amplitude mode profile and effective velocity along the waveguide. A single-mode waveguide supports only one guided mode at each operating wavelength. A single-mode waveguide, in which the optical intensity profile across the waveguide has a single maximum with an approximately exponential fall-off outside the waveguide, can be made using a relatively narrow and shallow channel. The mode width decreases with increasing refractive index difference. To efficiently couple light between a dielectric waveguide and a fiber butted against it, the optical modes of the two structures have to be made as similar as possible. The field mismatch can be reduced by adjusting the core dimensions and/or the refractive indices of the core and cladding [17].

2.2 GENERAL DESIRABLE PROPERTIES:

Several properties are desirable in the material selected for the waveguide, depending on its applications. The optical waveguide material must possess these salient parameters:

(a) **Waveguide modes**

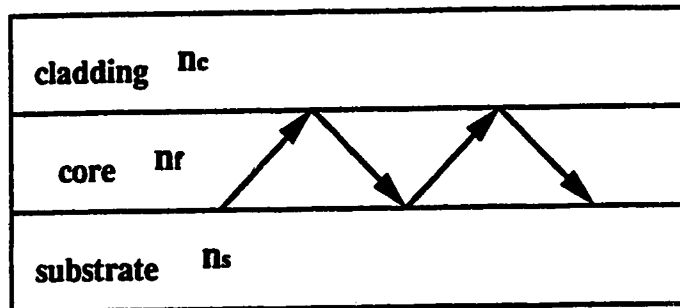

(b) **Substrate modes**

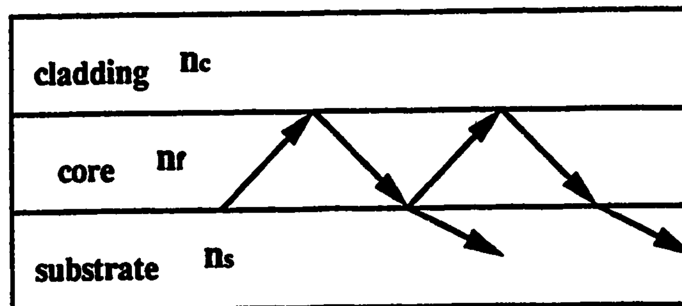

(c) **Substrate-cladding modes**

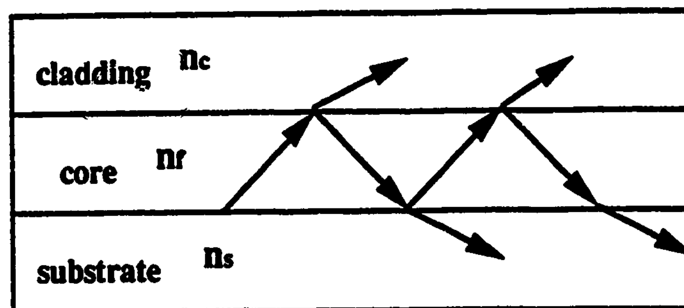

Figure 2.1 Different types of possible modes when $n_f > n_s, n_c$

(i) **Thermal stability:** The material must be able to withstand high annealing temperatures of 800°C-1200°C and still maintain its optical, mechanical and physical properties.

(ii) **Environmental stability:** The material must be reliable under a variety of environmental conditions such as high humidity and thermal adhesion stress.

(iii) **Low optical loss:** Although the length of the optical waveguide links are anticipated to be relatively short (less than several cm) it is important to develop the lowest loss material possible (< 1 dB/cm).

(iv) **Film quality:** The films should be smooth, free of striations and defects, and of a well controlled thickness. It should be also capable of forming a stable, uniform, well adhering and preferably amorphous hard glass-like material.

(v) **Refractive index:** Both the core and cladding layers require a precise control of refractive index.

(vi) **Process integration:** The material and process must be compatible with the chosen substrate and reproducibility is necessary. It should be easy to etch by standard photolithographic techniques.

Some popular materials [2] used are the polymeric materials such as polyurethane, epoxy, photoresist (PR) and polymethyl methacryalate (PMMA), and glass materials such as soda-lime glass, pyrex (Corning) glass and fused quartz, and chalcogenide compounds, lithium niobate ($LiNbO_3$), lithium tantalate ($LiTaO_3$), zinc oxide (ZnO), silicon nitride (Si_3N_4), tantallum oxide (Ta_2O_5) and niobium oxide (Nb_2O_5). The SiO_2/Si substrates can be used as a substrate for thin film waveguides. The thermal or chemical vapor deposited (CVD) silicon dioxide can be used as the core or buffer or cladding material.

The waveguide width, depth and the refractive index difference between the waveguide and the substrate, the three parameters that control the waveguide properties, can be separately controlled in the fabrication process. The fabrication technique chosen must not introduce surface roughness or volume defects because these result in scattering which in turn causes attenuation and limits throughput. To meet the desired specification of the waveguide characteristics of a given material, an appropriate fabrication technique is selected. Several fabrication techniques are thermal diffusion, ion exchange, ion implantation, polymerization, flame hydrolysis, epitaxial growth (e.g. vapor phase epitaxy and liquid phase epitaxy) and deposition methods (such as spin and dip coating, vacuum evaporation, RF or DC sputtering and chemical vapor deposition) [2].

A measure of the waveguide loss is a critical parameter in evaluating whether a waveguide structure may be adequate for applications in optical interconnects. This refers to the attenuation of the propagating modes excited by the incident radiation and not the large initial loss from the excited radiation modes (see for example Fig. 4.7). Waveguides with losses less than 1 dB/cm are adequate for the relatively short (several cm) distances in which these structures are to be used [18]. Losses may be due to scattering centers or coupling between fiber and waveguide or absorption by the substrate. Most of the scattering losses are known to originate from surface imperfections in the guides. The scattering losses are large at the glass/air interface and this could be reduced by suitably cladding the waveguide. There is also the coupling loss which is due to the launch conditions rather than the waveguide characteristics. The power coupling into a waveguide is a strong function of how the light is launched. The waveguide end faces, which may have chips, digs and scratches, are to be prepared for efficient coupling by conventional polishing. Absorption loss is due to light absorption by the substrate material. The absorption losses due to the silicon substrate are made negligible by providing a sufficient buffer layer to prevent any evanescent coupling of light.

2.3 WAVEGUIDE CLASSIFICATION:

A waveguide is classified according to its geometry as either slab or channel.

(a) Slab waveguides:

The waveguide in which the light confinement is along the depth (x-direction) is a slab or 2-D optical waveguide as shown in the Figure 2.2. There are two different types based on the refractive index profile as shown in the Figure 2.3.

(i) A **step-index waveguide**, in which the refractive index changes abruptly between layers.

(ii) A **graded-index waveguide**, in which the refractive index changes continuously with the depth.

Since the light is confined in the x-direction only, a light beam in a slab waveguide expands due to diffraction during propagation. Slab waveguides can be fabricated by deposition techniques such as sputtering, chemical vapor deposition, flame hydrolysis and evaporation, ion exchange and ion implantation, spin and dip coating, etc. Some waveguiding materials such as Si_3N_4, Ta_2O_5, Nb_2O_5 and barium silicate have exhibited losses less than 1 dB/cm after laser annealing [19]. Silicon nitride films (Si_3N_4) thin film optical waveguides with propagation losses of less than 0.1 dB/cm for the TE_0 mode at λ_0=6328 Å have been successfully grown by low-

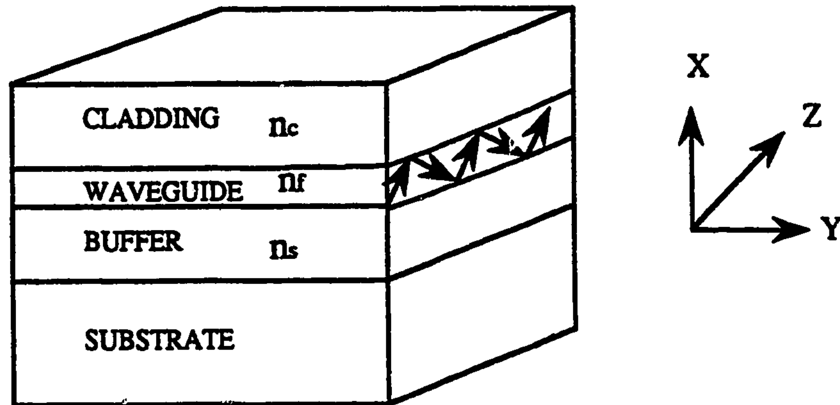

Figure 2.2 Slab waveguide

(i) Step index profile

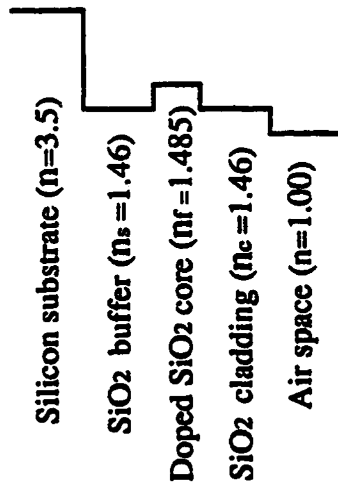

(ii) Graded index profile

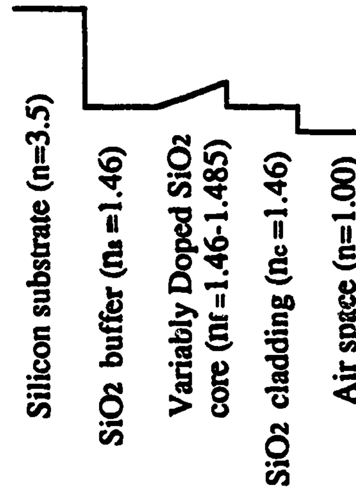

Figure 2.3 Different types of refractive index profiles

pressure chemical vapor deposition [20]. Deposited ZnO and Corning 7059 glass which were subsequently laser annealed (to reduce the scattering loss introduced by the fabrication process) showed the lowest value of loss that has been achieved on the silicon substrate. Laser annealed ZnO showed a loss of 0.01 dB/cm [21] while 7059 glass showed a loss of 0.05 dB/cm which was further reduced to 0.01 dB/cm by applying a surface coating [22].

Slab waveguides also have been made using phosphorus-doped silicon dioxide. The presence of phosphorus increases the refractive index of the glass. Measurements showed that an undoped thick layer (~15 μm) of silicon dioxide had a loss of 0.5 dB/cm [23]. By using phosphorus doping the oxide layer was reduced to about 6 μm with a loss of 2.3 dB/cm at a wavelength of 0.488 μm. Thermal or laser annealing further reduced the losses of phosphosilicate glass to less than 1 dB/cm [24]. Doped, deposited oxide can be reflowed to produce graded-index profile and low-loss slab waveguides [25]. Waveguides with strong field confinement using graded-index films have been fabricated by oxidizing silicon wafers under time-varying conditions [26]. The refractive index of SiO_2 was dependent on the growth temperature and the water content of the ambient oxygen during the oxidizing process. By varying these two quantities a multi-layered slab waveguide of gradually varying refractive index was developed with losses as low as 0.6 dB/cm at moderate thicknesses.

Other slab waveguides on silicon have been demonstrated. Thermal nitridation of oxidized silicon has produced waveguides with losses less than 0.1 dB/cm at a wavelength of 0.633 μm [27]. Single-mode oxynitride waveguides 0.1 μm thick are formed on the oxide surface with a loss of less than 1 dB/cm [28]. High-silica slab waveguides formed by flame hydrolysis deposition exhibit a loss of 0.1 dB/cm at a wavelength of 0.6328 μm [29]. Antiresonant reflecting optical waveguides (ARROW) in Si-SiO_2 multilayer structures have been fabricated with a low-loss of 0.4 dB/cm in the TE_0 mode and 60 dB/cm in the TM_0 mode thus showing a good polarization discrimination [30]. Low-loss slab waveguides in fused silica using nitrogen implantation are available with a loss of 0.1 dB/cm after annealing [31]. Optical losses of 1 dB/cm have been reported for slab waveguides of organic compounds with indices greater than that of silicon dioxide [32]. In chapter 3 of this thesis, we describe the fabrication of single-mode phosphorus-doped glass slab waveguides on silicon.

(b) Channel waveguides:

A waveguide in which the light is laterally confined in the y-direction in addition to the confinement along the depth (x-direction) is a channel or 3-D optical waveguide. Light confinement in the y-direction is required to achieve efficient light modulation and switching. Channel waveguides are classified according to their structure into different types as shown in the Figure 2.4.

(i) **Ridge:** Ridge channel waveguides are formed by the removal of undesired higher-index film from the substrate with dry etching and the lift-off of the deposited film. Ridge waveguides have strong transverse confinement of light but their shortcoming is significant scattering loss due to waveguide wall roughness.

(ii) **Voltage-induced:** This particular type of waveguide is formed by placing planar electrodes on slab waveguides of electro-optic crystals such as $LiNbO_3$ and $LiTaO_3$, and works by using a voltage-induced refractive index change to define a waveguide channel.

(iii) **Loaded:** This type includes channel waveguides both with dielectric loading and metal loading. By cladding a dielectric film, the effective index of the guided mode becomes higher; on the other hand the metal cladding gives a considerable reduction of the effective index.

(iv) **Buried:** Higher-index guiding layers are formed near the substrate surface by metal indiffusion, ion exchange and ion implantation. The buried type of channel waveguide has the advantage of low propagation losses with a very smooth surface.

(v) **V-groove or "Nabla":** This type of structure is formed by anisotropic etching of silicon. The higher index region is imbedded within the buffer layer. Higher index layers are formed by deposition of glass, phosphosilicate glass, polymers and other dielectric films. The propagation loss is low due to smooth wall surfaces.

Substantial progress has been made in both expanding the available materials and improving the optical performance of channel waveguides. Examples include ion exchange in glasses, diffusion of titanium in $LiNbO_3$, epitaxy of GaAs and GaAlAs, thin film deposition (CVD, electron-beam evaporation, sputtering, coating) of glasses, metal oxides, silicon nitride as well as a range of polymers. In many cases the losses of these materials are below 1 dB/cm [2]. There are several approaches to fabricating low-loss channel waveguides using silicon dioxide (SiO_2) on silicon substrates. The propagation loss of a sputter-deposited zinc oxide on the chemically etched ridge of thermally oxidized silicon was greater than 10 dB/cm [33]. Losses in the ridge channel waveguide, 15 μm wide made using phosphosilicate glass are reported to be 1 to 2 dB/cm at 0.5145 μm wavelength after annealing [34]. The higher loss in ridge

(i) **Ridge**

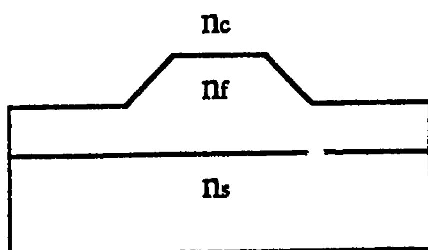

(ii) **Voltage induced**

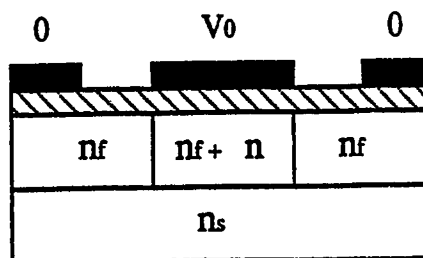

(iii) **Loaded**

(a) **Dielectric**

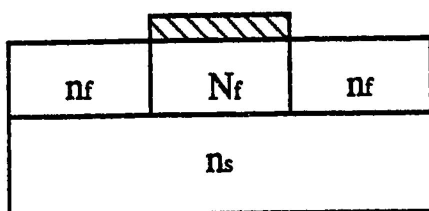

(b) **Metal**

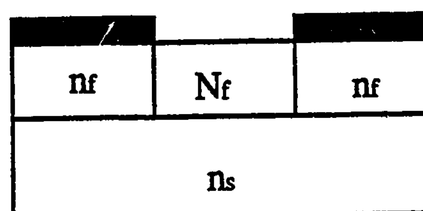

(iv) **Buried**

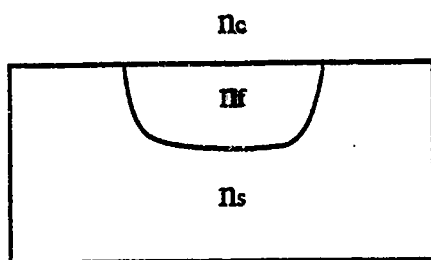

(v) **V-groove or "Nabla"**

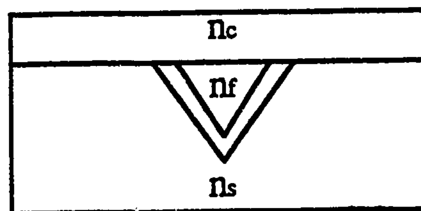

Figure 2.4 Different types of channel waveguides

guides are due to the difficulty in maintaining straight smooth edges during lithography and etching. Buried channel waveguides were fabricated using chemical vapor deposition (CVD) silicate glasses [35]. Phosphosilicate glass (PSG) has been deposited on a thermally oxidized silicon substrate and patterned into channels. A layer of borosilicate glass was deposited to form a cladding.

Henry *et al.* [36] have developed a low-loss waveguide of Si_3N_4 core surrounded by silica glass layers to provide a highly confined optical mode for proximity coupling to the channel substrate buried heterostructure lasers. An acid etch was used to define the Si_3N_4 rib structure on the oxidized silicon prior to the deposition of a TEOS glass layer. Waveguide losses below 0.3 dB/cm were measured in the 1.3-1.6 mm wavelength range. Henry *et al.* [3] also designed a waveguide to match an optical fiber. The waveguide has a p-glass core on a HIPOX base layer and was covered with a cladding layer of glass. The core was 4-5 mm thick and 7 mm wide, doped with 6.5-8 wt. % phosphorus and flowed into a bell shape during annealing. The waveguide loss was measured as low as 0.05 dB/cm and the fiber coupling loss was 0.5 dB for a wavelength of 1.5 mm. Valette *et al.* [37,38] developed two waveguides with low-losses. The first was a Si_3N_4 core surrounded by SiO_2 with lateral confinement achieved by etching a rib on the top surface. The second waveguide was a ridge channel guide of doped SiO_2 surrounded by SiO_2. All layers were deposited by plasma-enhanced chemical vapor deposition. Low-loss, single-mode channel waveguides on silicon have also been made by imbedding a core ridge waveguide in a glass cladding layer. Takato *et al.* [39] have fabricated the glass buffer, core and cladding layers by flame-hydrolysis and the rectangular core was formed by reactive-ion etching. The loss for a 8 mm^2 core was in the 0.1 to 0.2 dB/cm range.

Anisotropic etching of silicon has previously been used to form trench waveguide structures. The waveguide materials used to fill the etched V-shaped grooves and buffered imbedded channels were dielectrics like the epoxy [40], plastics [41,42] and sputtered 7059 glass [43]. Sputtered glass waveguides have also been formed in deeply etched vertical grooves of silicon [43]. Losses of trench waveguides on silicon substrates have generally been in the range of 2-4 dB/cm [25]. Lower transmission loss levels will likely be achieved by better waveguide formation techniques. In our laboratory, low-loss polymer waveguides using Norland 81 optical adhesive have been made in silicon V-grooves [44]. In chapter 4 of this thesis, we describe the fabrication of CVD phosphorus-doped glass waveguides in silicon V-grooves which we call "Nabla" waveguides.

3. SLAB WAVEGUIDES

3.1 DESIGN:

The choice of material for the buffer, core and cladding layers of our waveguides are dictated by the materials readily available in the silicon industry and our laboratory. The single-mode, phosphorus-doped glass slab waveguides fabricated on silicon were made up of three layers:

(i) Silicon dioxide as the buffer layer: A guided wave leaks through the silicon dioxide layer into the silicon substrate because the refractive index of silicon is larger than the refractive index of the guiding layer. To reduce this leakage loss to an acceptable value, the thickness of the silicon dioxide buffer layer must be larger than the depth of the guided-wave penetration into this layer. The necessary silicon dioxide thickness depends upon the refractive index and thickness of the waveguide film, as well as the guided-wave wavelength and mode. This buffer layer must be thicker for smaller differences in refractive indices between the guiding and the buffer layer. The leaky waveguide losses increase as the silicon dioxide buffer layer thickness decreases. Generally speaking, the thickness of the buffer layer must be at least a few optical wavelengths to prevent tunneling from the waveguiding layer to the substrate.

(ii) Phosphosilicate glass (phosphorus-doped glass) as the core: Most of the light propagates in the core which has a higher index than the surrounding layers. The exact thickness of the waveguide core depends on the wavelength of light to be guided, the refractive index difference and the desired number of modes. The core refractive index should not be too close to that of the underlying layer of silicon dioxide, nor should it be too high [45]. If the refractive index is too close to that of silicon dioxide, a considerable attenuation may be experienced due to evanescent wave coupling between the waveguide core and the highly absorbing silicon substrate, unless the silicon dioxide buffer layer is very thick. On the other hand, if the index is too high (>2), there will be a strong reflection loss at the waveguide-fiber junction. Reflection loss at the waveguide-fiber junction can be minimized by using a thin film waveguide core having a refractive index close to that of the fiber core.

(iii) Silicon dioxide as the cladding layer: One of the most important factors limiting the performance of the integrated optical devices is the scattering of light in the waveguide. The waveguide fabrication procedure must be optimized to reduce scattering to a minimum. The cladding film deposited on the core reduces the scattering losses in the waveguides by reducing the effect of surface irregularities.

The standard theory [2] is used in designing the single-mode slab waveguides. The design is discussed in detail in the Appendix 1. The two important parameters of the slab waveguide are the numerical aperture and thickness. The guiding layer is made up of phosphorus-doped glass and the index of refraction is 1.485 for 10 wt. % doping as extrapolated from the Figure 3.1. A flow rate of 1 cc/min. of phosphine resulted in a phosphorus content of 1 wt. % in the silicon dioxide. The waveguides contained 10 wt. % of phosphorus, as investigation on this value of doping percentage was carried out earlier [46]. The index of refraction of the silicon dioxide buffer and cladding layer is 1.46. The waveguides have a step-index of refraction with a numerical aperture of 0.27. The maximum thickness of the guiding layer for only the fundamental mode to propagate is calculated to be 1.16 μm. The estimated thickness of the buffer layer is 4.5 μm and the cladding layer is 3.0 μm.

3.2 FABRICATION:

Silicon wafers {<100> orientation, Dopant- P (Boron), Resistivity- 1 to 10 ohm-cm, Diameter- 98.5 - 101.2 cm, Thickness- 457 - 559 μm} were used as substrates for the slab waveguides. The silicon substrates are etched in dilute hydrofluoric acid, cleaned in a *"piranha"* solution (1800 ml sulfuric acid and 600 ml of hydrogen peroxide), rinsed in deionized water and dried to obtain an oxide-free clean substrate. The silicon wafers are then loaded in the low-pressure chemical vapor deposition (LPCVD) chamber. The silicon dioxide films are deposited by the oxidation of silane at 430°C in the nitrogen (N_2) ambient. A film of 4.5 μm silicon dioxide was deposited as the buffer layer. The doped glass film was grown by the co-oxidation of silane and phosphine gas at 430°C in presence of the N_2 carrier gas. The silane and phosphine gas are diluted in argon before being fed to the chamber. The phosphorus-doped glass layer was 1 μm thick. The refractive index of the phosphorus-doped oxide layer can be varied by changing the phosphine flow rate. Finally, a cladding film of 3 μm silicon dioxide was deposited. The phosphorus-doped glass slab waveguide is as shown in the Figure 3.2.

The low-pressure chemical vapor deposition process produces thick films of excellent quality without any evident cracks. Heat treatment subsequent to the deposition of the film has a marked effect in decreasing the losses [35]. Annealing at elevated temperatures leads to the densification of the film, relieving of strain and sintering of glassy particles resulting from gas phase nucleation during the CVD process. Phosphosilicate glass reflow also helps in reducing the surface roughness that causes high scattering losses. The wafers with the CVD films are subjected to

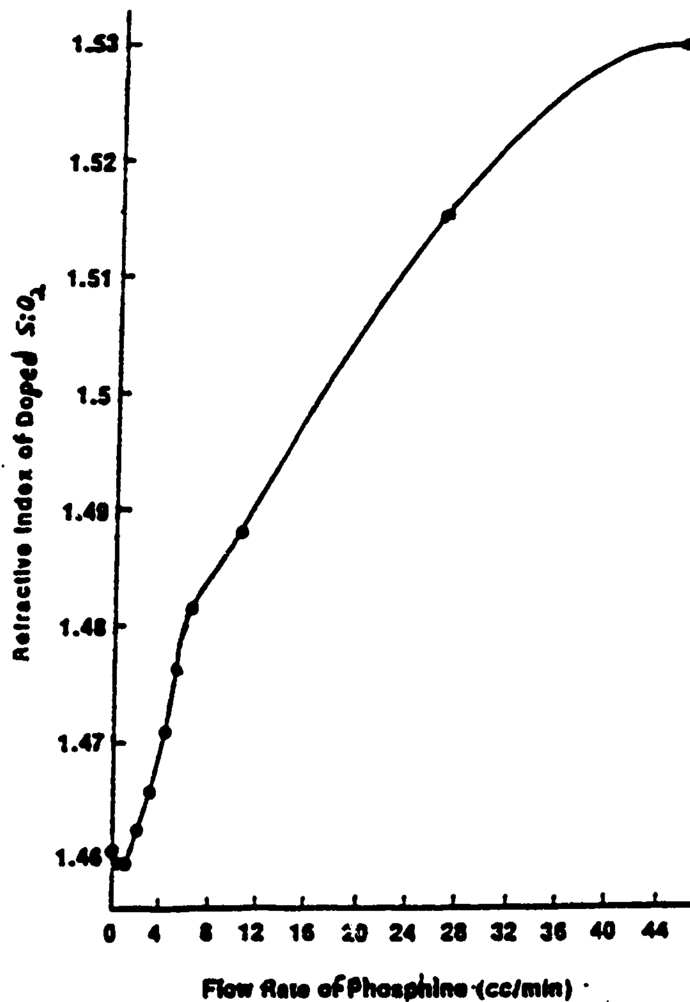

Figure 3.1 Refractive index (n) of the doped SiO_2 vs. the phosphine flow rate (cc/min). A flow rate of 1 cc/min resulted in a phosphorus content of 1 wt. % in the SiO_2.

(From "Si-based integrated optics technologies", S. Valette *et al.*, Solid State Technology, February 1989.)

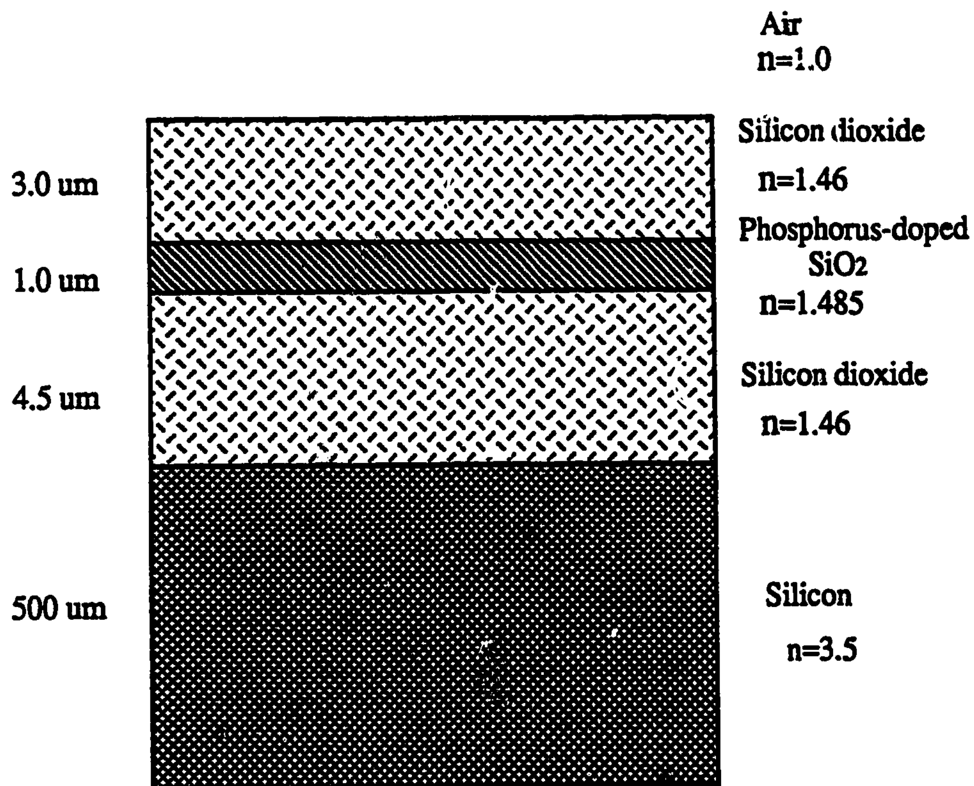

Figure 3.2 Phosphorus-doped glass slab waveguide.

1050°C, 120 minutes anneal in the nitrogen ambient to provide a dense, stress-free and defectless wafer. It was found by using "SUPREM III" [47] (a program for integrated circuit process modeling and simulation developed at Stanford University) that there is very little diffusion of the phosphorus into the buffer and cladding layers (with a rise in temperature) so that the step-index profile remains intact (see Figure A.1.2). Details of the calculation are given in the Appendix 1.

3.3 LOSS MEASUREMENT:

The light source used in all the experiments is a 10 mW helium-neon (He-Ne) laser with a beam diameter of one millimeter and a wavelength of 0.6328 μm. This particular wavelength is chosen due to the fact that its light was visible to the naked eye. This makes the observation of the waveguide properties quite simple. The set-up used to measure the scattered light as shown in the Figure 3.3 involves a chopper (with a frequency of 200 Hz) linked to a lock-in amplifier, which effectively nullifies the effects of the 60 Hz background light by controlling the laser beam. A silicon photodetector is also connected to the lock-in amplifier. A plastic fiber with a numerical aperture (NA) of 0.5, in turn connected to the photodetector, is used as collector of the scattered light. The measurement recorded is in the form of percentage relative to the adjustable maximum setting of the lock-in amplifier.

The waveguide samples are in the form of a 4 inch diameter wafer. The silicon wafers with the deposited CVD oxide layers are diced into long pieces with flat edges. The end-face of the wafer upon which the light is shone is polished to decrease the amount of light scattered due to the edge roughness. The edges are polished on a glass plate with 1 μm grit size and water as the lubricant. The polished end helps in increasing the amount of light launched into the waveguide. Optical measurements were performed using end-fire coupling. The light from the helium-neon laser is shone on the end facet of the waveguide sample. The brightness of a guided wave streak is proportional to the guided light intensity at each point provided the waveguide is uniform. Measurement of the scattered light intensity distribution along the propagation of a guided wave enables the determination of the propagation loss. The spacing between the fiber end-face and the waveguide surface must be kept constant. The fiber is held at right angles to the waveguide and scanned along its length so that a plot of the relative scattered optical power versus length can be made.

The loss per unit length is determined from the slope of this curve. This technique of loss measurement implicitly assumes that the scattering centers are uniformly distributed and the intensity of the scattered light in the transverse direction

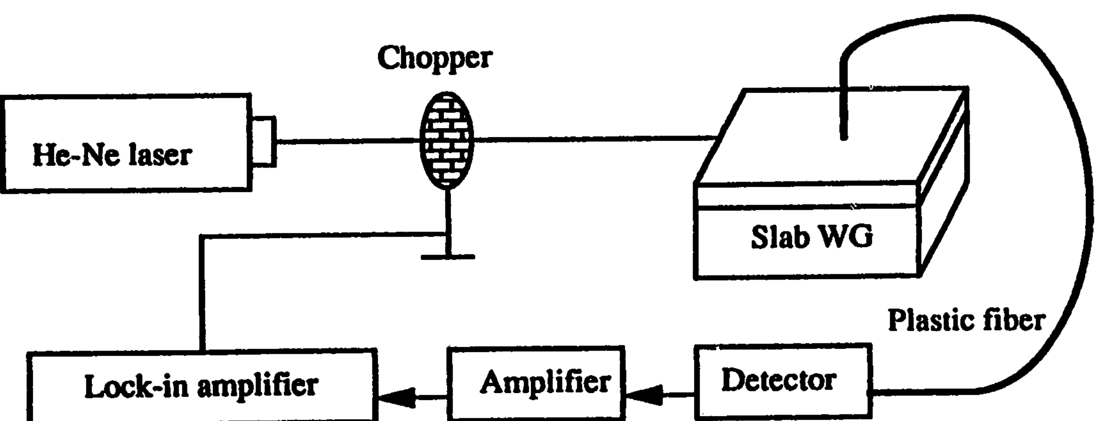

Figure 3.3 Set-up for measuring slab waveguide scattering losses

is proportional to the number of the scattering centers. In that case, it is not necessary to collect all the scattered light, but the spacing between the fiber and the waveguide be kept constant. This scattering loss detection method, being non-destructive, is used most often to measure losses in thin film waveguides. The loss measurements were carried out for many waveguide samples. The scattered light intensity measurements (in %) are recorded for each point moved along the waveguide and the slope of the plot of the log of scattered light intensity and distance gives the attenuation for the waveguide sample. The loss is less than 0.1 dB/cm for all the samples measured as shown in the Figure 3.4. The loss data and the graphs are attached in Appendix 4. The samples without the glass cladding gave a loss of 0.8 dB/cm [46], so we can conclude that the glass cladding reduced the losses considerably. Also, without annealing the samples, the losses were as high as 2.6 dB/cm, as shown in the Figure 3.5. Thermal annealing has brought down the losses to a very low value.

PHOSPHORUS-DOPED GLASS SLAB WAVEGUIDE-1

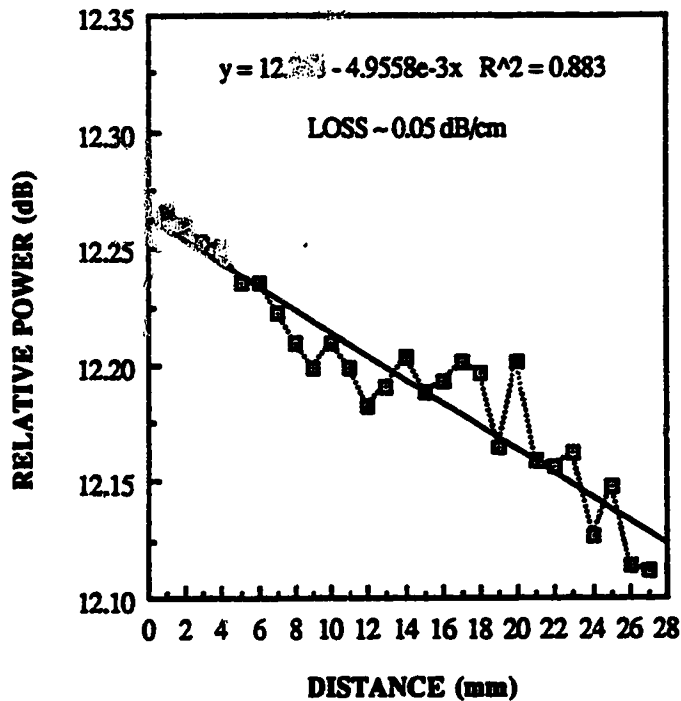

PHOSPHORUS-DOPED GLASS SLAB WAVEGUIDE-2

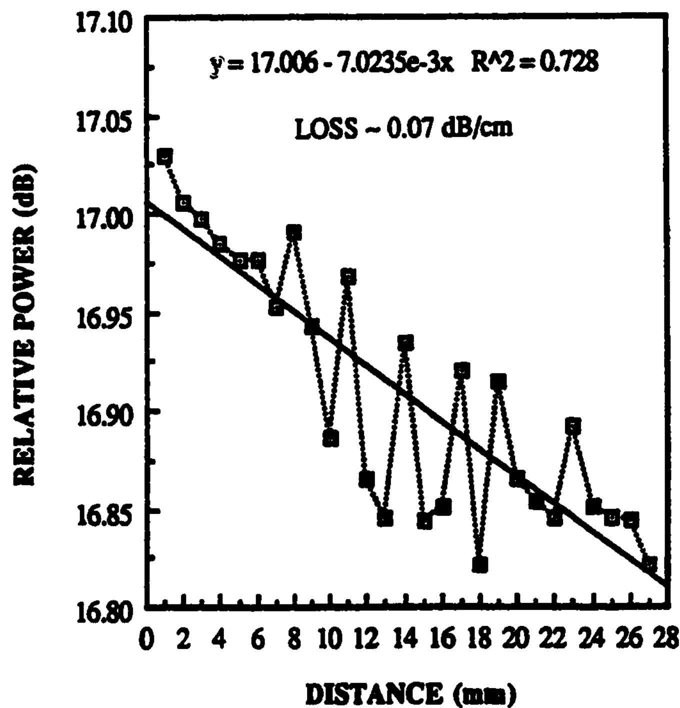

Figure 3.4 Attenuation plots of annealed phosphorus-doped glass slab waveguides.

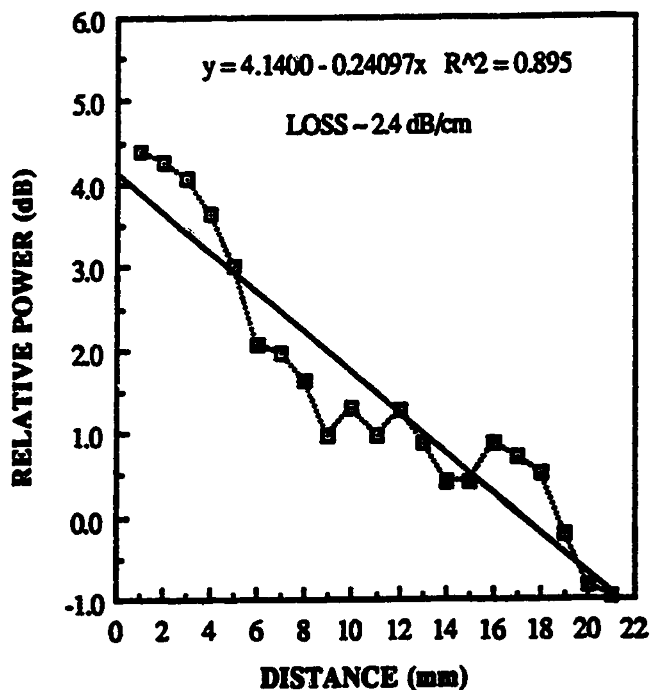

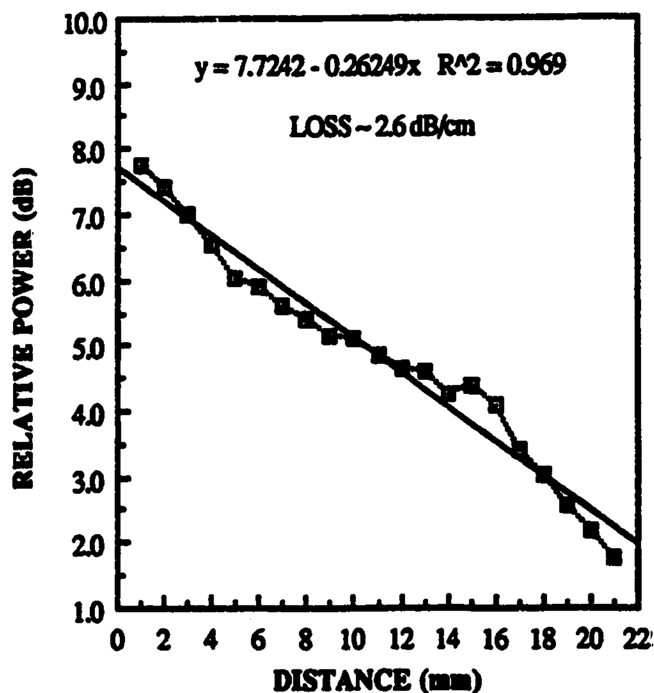

Figure 3.5 Attenuation plots of unannealed phosphorus-doped glass slab waveguides.

4. NABLA WAVEGUIDES

4.1 DESIGN:

The single-mode channel waveguides fabricated in silicon V-grooves are made up of three layers, namely, silicon dioxide as the buffer layer, phosphosilicate glass as the core and silicon dioxide as the cladding layer {see Figure 2.4 (v)}. The design considerations of the single-mode nabla waveguides, based on the triangular waveguide being compared to the cylindrical single-mode fiber, are discussed in the Appendix 2. This design gives the approximate values for the core thickness in order to achieve single-mode propagation. The numerical aperture is similar to that of the slab waveguide. The maximum width and depth of the guiding layer for only the fundamental mode to propagate is 1.88 μm and 1.33 μm respectively. The estimated buffer layer thickness is 4.5 μm and the cladding layer thickness is 3 μm. The cladding layer also provides a smooth surface geometry which reduces scattering losses. It is difficult to perform an accurate design because there is no theory for triangular geometry of the nabla waveguide.

4.2 FABRICATION:

(a) GENERAL PLAN:

The original plan was to deposit a 4.5 μm thick buffer layer and a 1.0 μm thick phosphorus-doped oxide layer and then to polish away the extra material on the surface outside the groove. However, it was found that hand polishing caused material to be dug out of the groove and roughened the surface. Grinding and polishing was tried on an Ecomet 3 grinding/polishing machine using various grades of silicon carbide (SiC) polishing paper and alumina powder. Polishing was tried for days without any progress. Two samples were also sent to the Buehler Lab in Chicago. A better polishing method could not be suggested by them as the oxide layer was too hard to polish with a small tolerance of 0.1 μm.

Then the method of filling the grooves with thick layers of CVD silicon dioxide was tried. Thicker layers of silicon dioxide are more likely to crack. Both cracks and pinholes can be revealed by scanning electron microscopy (SEM) or by subjecting to immersion in an etchant which etches the material [48]. There were very evident cracks in the thick oxide layers which couldn't be removed even after annealing three times for 150 minutes at 1050°C in N_2 ambient. The cracks were assumed to be either due to the shadow deposition or due to the growth of a thick CVD oxide on the PSG layer. The latter proved to be true as it was due to the fact that the tensile stresses

are greater in the case of pure CVD oxide which causes the film to crack when thicker films are deposited.

Deposited SiO_2 films when heated above the deposition temperature are put in additional tension. There is some correlation between the intrinsic tensile stress in deposited films and the temperature increment above deposition temperature which can be attained before the cracks begin to form [48]. Another consequence of film stress is film cracking which occurs due to a difference in the thermal expansion coefficients [49]. The thermal coefficient of expansion of silicon dioxide is lower than that of silicon, therefore increases in temperature result in increases in tension or decrease in compression depending upon the initial stress condition of the film. Since low temperature SiO_2 films are in considerable tension when deposited, they are susceptible to cracking during increases in temperatures. These cracks caused underetching of the material in the groove as shown in the Figure 4.1 when the etch-back procedure in 10:1 BOE was tried. The etch rate of pure CVD oxide is 0.1 µm/minute after annealing.

The next feasible method of depositing thicker layers of phosphorus-doped glass (PSG) in silicon V-grooves was tried. A thick layer of PSG is deposited to fill the waveguide groove so that an etch-back procedure could be used to get rid of the extra doped material on the sides of the groove without removing the material in the groove. The doped oxide was etched till the required core shape and size was obtained. The outline of this fabrication process is as shown in the Figure 4.2. This method involving the following steps was adapted successfully to fabricate nabla waveguides.

(b) FABRICATION DETAILS:

(i) Substrate preparation:

Silicon wafers {<100> orientation, dopant- P (boron), resistivity- 1 to 10 ohm-cm, diameter- (98.5 - 101.2 cm), thickness- (457 - 559 µm)} are used as substrates for the channel waveguides. The silicon substrates are cleaned using a *"piranha"* solution (1800 ml sulfuric acid and 600 ml hydrogen peroxide). Thermal oxide is grown on the silicon wafer using the Thermco furnace by bubbling nitrogen in water at 1050°C for 60 minutes. The thickness of the thermal oxide is about 0.5 µm. This layer of thermal oxide is used as the mask to transfer the waveguide pattern onto the surface of the silicon wafer.

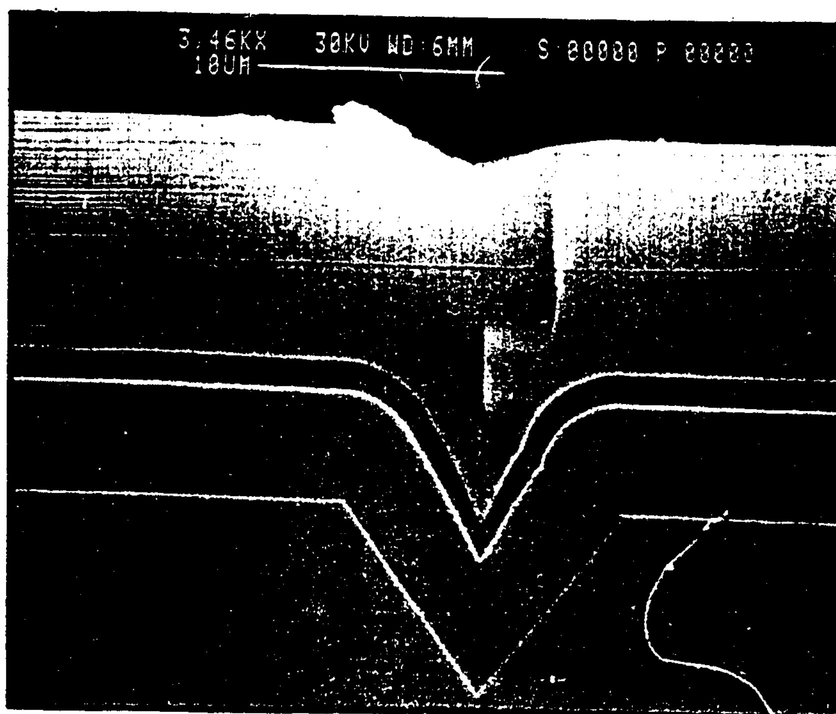

Figure 4.1 (a) Silicon V-groove with 4.5 mm silicon dioxide, 1 mm phosphosilicate glass and 8.0 mm silicon dioxide.

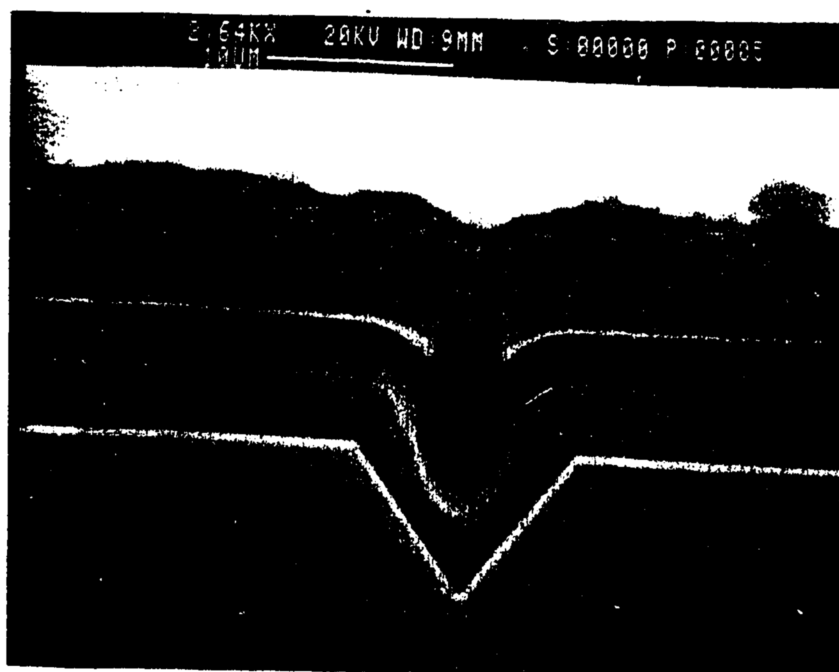

Figure 4.1 (b) Under-etching of the oxide due to the crack.

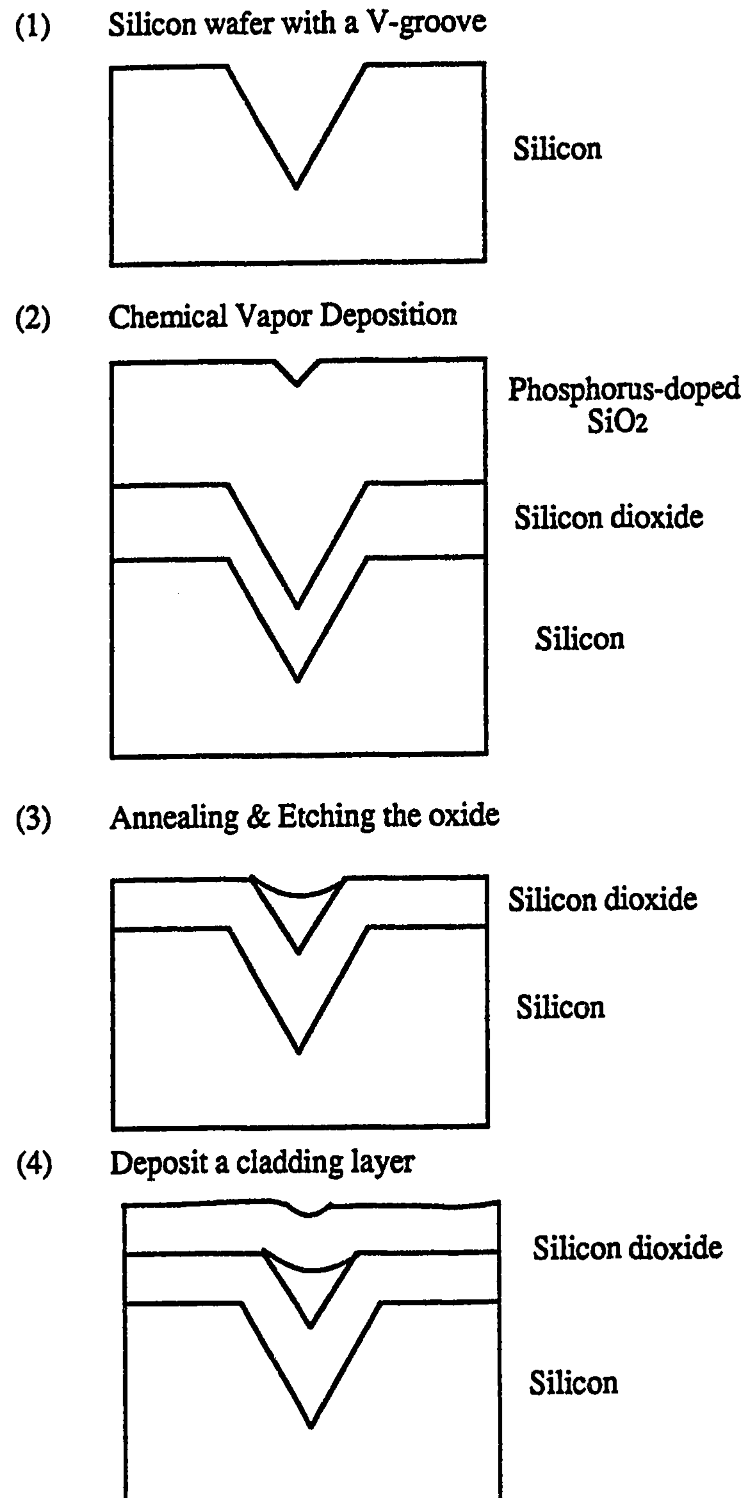

Figure 4.2 Fabrication of the phosphorus-doped glass nabla waveguides.

(ii) Photolithography:

The next step is the photolithographic technique used to transfer a pattern from a master photomask to the oxide mask. A thin layer of HPR-204 positive photoresist is spun on the oxide surface using the Solitec spinner at a spin speed of 3500 rpm for 15 seconds. The layer of photoresist is pre-baked or soft baked at 110°C in vacuum for 50 seconds using the Solitec hot plate to vaporize the solvents completely and to enhance adhesion to the substrate. A photomask is placed in contact with the photoresist-coated surface and the wafer is exposed to 200 W ultraviolet lamp radiation for 11 seconds. The ultraviolet radiation causes a chemical reaction in the exposed areas of the photoresist. The wafer is then rinsed in the developing solution (Microposit developer 354) which removes the exposed areas of the photoresist leaving a pattern on the wafer surface. These wafers are post-baked or hard baked at 120°C in vacuum for 60 seconds using the Solitec hot plate to increase resistance against etching. The wafers are placed in a solution of 10:1 buffered oxide etch (BOE), which attacks the thermal oxide at the rate of 0.05 µm/minute in the exposed areas but does not attack the photoresist or the underlying silicon. The wafers are taped at the back to protect the oxide on the back of the wafer. Once the exposed oxide is etched away, the remaining positive photoresist is stripped using acetone. The final result is a pattern of oxide on the wafer surface that duplicates the photoresist pattern. The detailed recipe is discussed in the Appendix 3.

(iii) Anisotropic etching:

Anisotropic etchants, known as orientation-dependent or crystallographic etchants, etch at different rates in different directions in the crystal lattice. They can form well-defined shapes with sharp edges and corners. The type of hole an anisotropic etchant forms in a wafer is determined by the crystal orientation of the wafer surface as well as by the orientation dependence of the etchant [50]. Most silicon wafers have a flat edge parallel to a <110> direction. The photomask is lined up with this flat edge during the exposure step that precedes the etching. The size of the oxide pattern determines not only the area of the pit on the wafer surface but also the depth of the pit. The depth of the pit depends on the width of the mask opening. By tapering the width a variable depth region is created. If the opening in the oxide on a <100> wafer is rectangular, anisotropic etching creates a long trench rather than an inverted pyramid. The walls and the ends of the trench are {111} planes and if the etch goes to completion, the trench has a V-shaped cross-section. The {111} planes intersect the {100} plane at an angle of 54.74° [50].

The anisotropic etchant used is an EDP etchant composed of 750 ml of ethylenediamine, 120 g of pyracatechol and 240 ml of water [51]. This etch solution boils at approximately 118.7°C and provides residue-free etching above 100°C. The etch solution is placed in a jar in a bath of oil with a water-cooled reflux condenser attached to the jar. The solution is stirred and maintained at 115°C and the wafers are etched at 0.8 to 1.0 μm/minute. The detailed recipe is discussed in the Appendix 3. The oxide is used as a mask during EDP etching. Removal of the thin native oxide from silicon surfaces in 10:1 BOE prior to immersion in EDP is essential to ensure uniform etching. Etching control is best achieved with a fresh solution of EDP. The silicon wafers etched in this anisotropic etchant are rinsed in deionized water and then the oxide mask is stripped away using 10:1 BOE leaving behind V-grooves of 9.78 μm width and 6 μm depth. The wafer processing technique is as shown in the Figure 4.3.

(iv) Deposition of buffer layer and core:

The silicon wafers with the V-grooves are cleaned in the *"piranha"* solution for 10 minutes and then loaded in the low-pressure, low-temperature CVD chamber. A buffer layer of silicon dioxide is deposited by the oxidation of silane at 430°C in the N_2 ambient. A thick layer of phosphorus-doped glass is then deposited by the co-oxidation of silane and phosphine at 430°C in N_2 ambient. The layer of silicon dioxide deposited on the sides of the groove is about 4.5 μm thick and the PSG layer is about 9.5 μm thick as measured using the scanning electron microscope (SEM). Lacking other means of monitoring film thickness, scanning electron microscope examination of cleaved cross sections of the samples was used to determine layer thickness.

It was observed by Naumaan and Boyd [52] that PSG films deposited at 400°C using LPCVD with 5 wt. % phosphorus and thicker than 3 μm were unstable and flaked off within minutes of being taken out of the reactor. Some flaking was also exhibited by films with 8 wt. % and thicker than 10 μm. Films with greater phosphorus content did not show any tendencies to flaking or cracking. Also when the wafers were loaded side by side into the furnace, the PSG layer on the central wafer did not develop any cracks whereas layers on the outer wafers did. Apparently the outer two wafers decreased the thermal shock to the central wafer. The oxide and PSG films at our laboratory were deposited on the wafers with baffle wafers on either side to prevent thermal shock and to maintain uniform deposition, uniform temperature and uniform gas flow. No flaking was observed for any of the 10 wt. % phosphorus-doped and 9.5 μm thick PSG film deposited as the waveguiding layer. Flaking cannot be tolerated as surface damage results in scattering losses. It is not easy to deposit

(1) Silicon Wafer

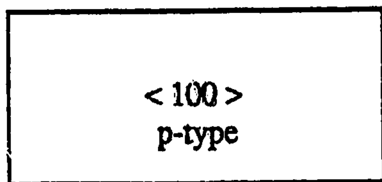

(2) Grow Thermal Oxide

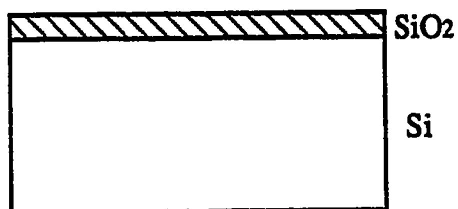

(3) Spread Photoresist & Softbake

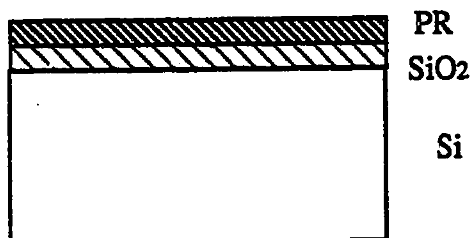

(4) Align, Expose & Develop

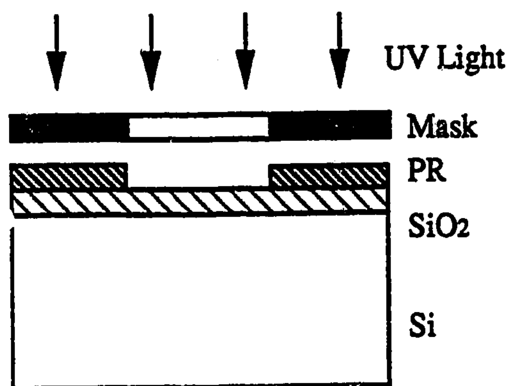

(5) Etch Oxide In B.O.E 10:1

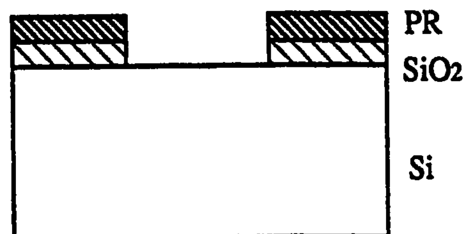

(6) Strip Photoresist

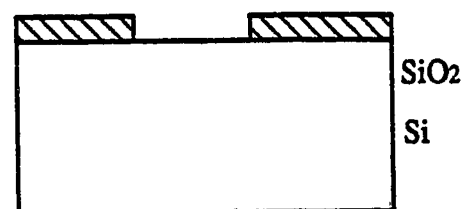

(7) Etch Si In E.D.P

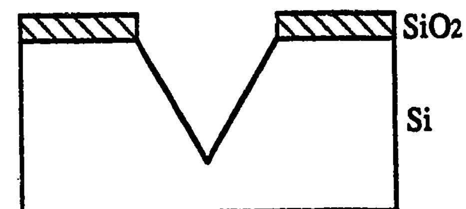

(8) Remove Oxide

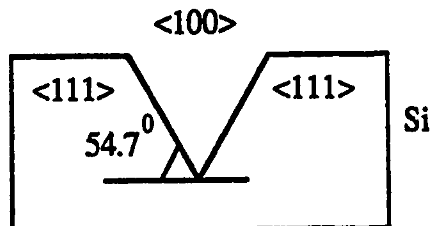

Figure 4.3 Wafer processing technique

films at higher phosphine flow rates due to the rapid gas phase reactions that exist at high phosphine concentration [53]. At higher phosphorus concentrations the uniformity in thickness and composition becomes degraded [54]. Also, PSG layers with excessively high phosphorus concentration tend to be hygroscopic and may have poor stability in a humid atmosphere [48].

The refractive index of the PSG film increases with increasing phosphine concentration [53]. At a given phosphorus concentration, the refractive index is greater for films deposited at higher temperatures, probably because the high temperature films are more dense [54]. The refractive index for a phosphosilicate glass film decreases with increasing wavelength [55]. Also the undoped glass after annealing at 1100°C had a refractive index very close to that of thermal oxide as the undoped glass densify when annealed at 1100°C. The refractive index and etch rate of a deposited film depends on the deposition conditions in addition to the dependence on phosphorus concentration. The deposition dependence can be removed by annealing the samples at 900°C for 30 minutes before the refractive index measurements and 800°C for 15 minutes for etch rate measurements [56]. The etch rate is uniform throughout the film; no variation with thickness was observed.

(v) Annealing and etching:

The maximum film thickness that can be attained is considerably greater for a PSG film than for a pure CVD oxide film. For a given growth rate and thickness the tensile stress is greatest for pure SiO_2 films and decreases with increasing phosphorus concentration [49]. The lower tensile stress in the PSG films is a significant advantage in terms of the maximum thickness that can be attained without causing the film to crack. Also the ability to reflow during annealing yields a dense film with no defects. The low temperature silane and oxygen process suffers from poor step coverage which can be remedied by flowing the glass at temperatures above 1000°C but flowing requires a relatively high phosphorus concentration, such as 6-10 wt. % phosphorus [54]. The layers for nabla waveguides were annealed at 1050°C for 150 minutes in nitrogen ambient (90% at 15 psi) using the Thermco Furnace.

The control of the oxide profile is achieved by doping the oxide to lower its softening point and annealing at a temperature above that point. For a given temperature, the viscosity is lowest for a steam ambient (highest flow) and greatest for a nitrogen ambient (lowest flow) with oxygen falling somewhere between the two [57]. An increase in the concentration of phosphorus in the oxide can change the viscosity-temperature characteristics of the film to cause flow at temperatures as low

as 1000°C. A given profile can also be achieved at a lower temperature but at the expense of a longer anneal time. The degree of glass flow is enhanced by increasing the phosphorus concentration, flow time, flow temperature, introducing water vapor in the ambient during the flow and increasing layer thickness [52]. Also the effects of the phosphorus diffusion into the oxide layer with resulting changes in phase composition need to be taken into account. The warping of the wafer due to the annealing is minimized by depositing the films on both sides of the wafer, which is possible in case of CVD process [58]. A large thermal gradient is created at the PSG-Si interface during the high temperature anneal and the resultant stress disrupts the integrity of the PSG layer [24]. The SiO_2 layer between the silicon and PSG provides a reduced thermal gradient at the PSG-SiO_2 interface which preserves the PSG layer.

The wafer with the buffer layer and thick layer of PSG is then dipped in a 10:1 BOE solution and the etch-back technique was tried which resulted in getting rid of the extra material on the sides of the groove. The etch rate of PSG in 10:1 BOE solution was found to be 0.3 μm/minute for a unannealed wafer and 0.08 μm/minute for an annealed wafer. This dramatic change in the etch rate is due to the densification of the film after annealing. Annealing of the PSG film results in a low-loss, fine structure and highly reliable film whose thickness decreases due to the densification [59]. The etch-back technique was carried out on many samples and each time the etch rate and etch time was the same. A better control was obtained by etching it slowly in the buffered oxide etch. The scanning electron micrographs of the etch-back technique of a single wafer for different etch times are shown in the Figure 4.4 (a-f). This etch-back process was repeated for five different samples. The etch time and the core geometry remained the same for all the samples.

The technique of fabricating optical waveguides by preferentially etching the V-grooves in a silicon substrate and then filling the grooves by deposition provides smooth waveguide walls. The waveguide is bounded by crystallographic walls which are structurally smooth. The self-limiting geometry obtained by the anisotropic etchant is an advantage in fabricating predictable device structures with a high degree of precision. Since the exposed surfaces are all bounded by crystal planes, the intersection angles between the various surfaces will be definite and the deposition of another layer of crystalline material on top of it should result in films of better quality and uniformity. Further, the waveguide profile can be controlled and reproduced with great accuracy. The repeatable results in controlling the required geometry is a useful aspect in large scale production.

Figure 4.4 Scanning electron micrographs of the etch-back technique.

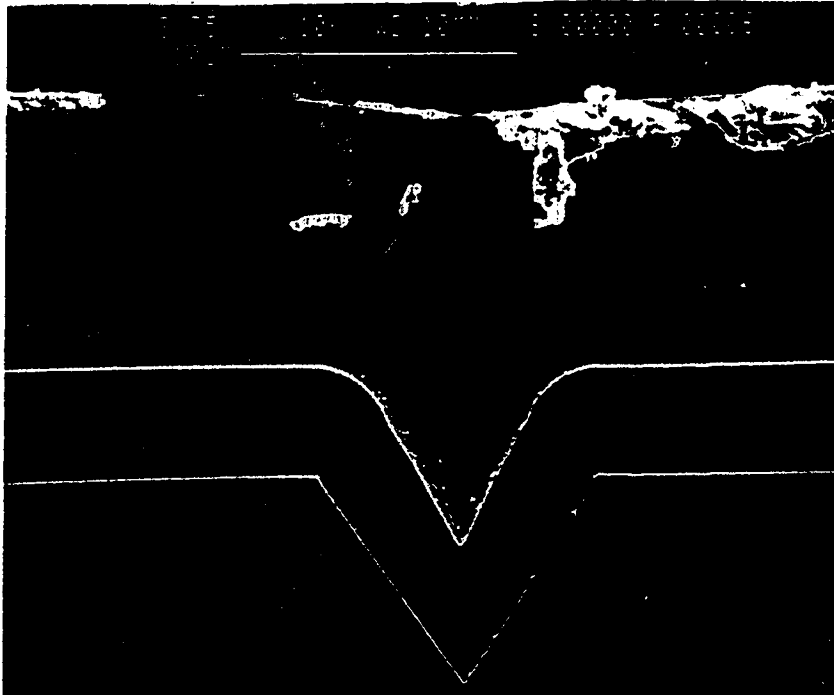

(a) Silicon V-groove with 3.8 mm silicon dioxide, 9.5 mm phosphosilicate glass.

(b) Silicon V-groove with 3.8 mm silicon dioxide, 3.8 mm phosphosilicate glass after 30 minutes BOE 10:1 etch.

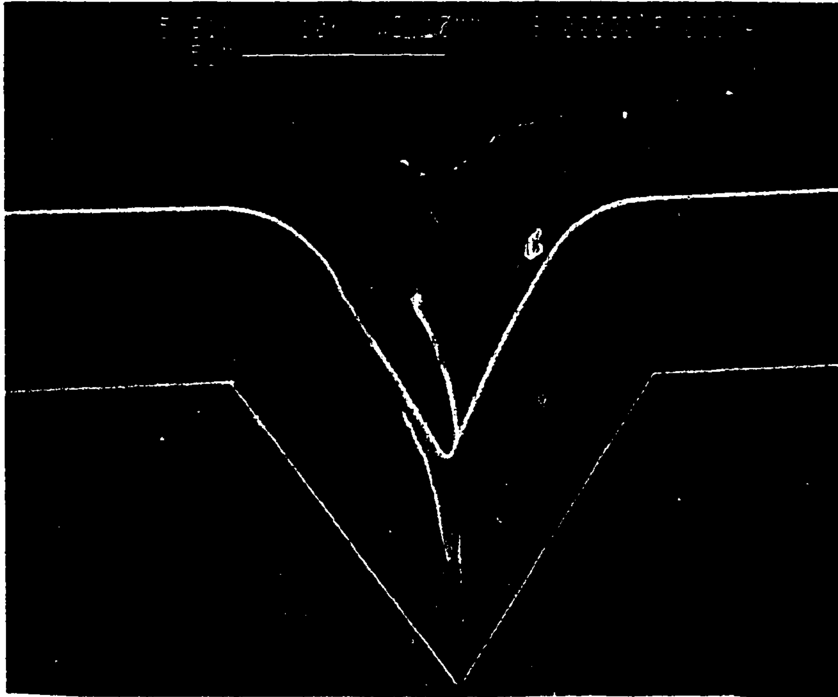

(c) Silicon V-groove with 3.8 mm silicon dioxide, 2.2 mm phosphosilicate glass after 45 minutes BOE 10:1 etch.

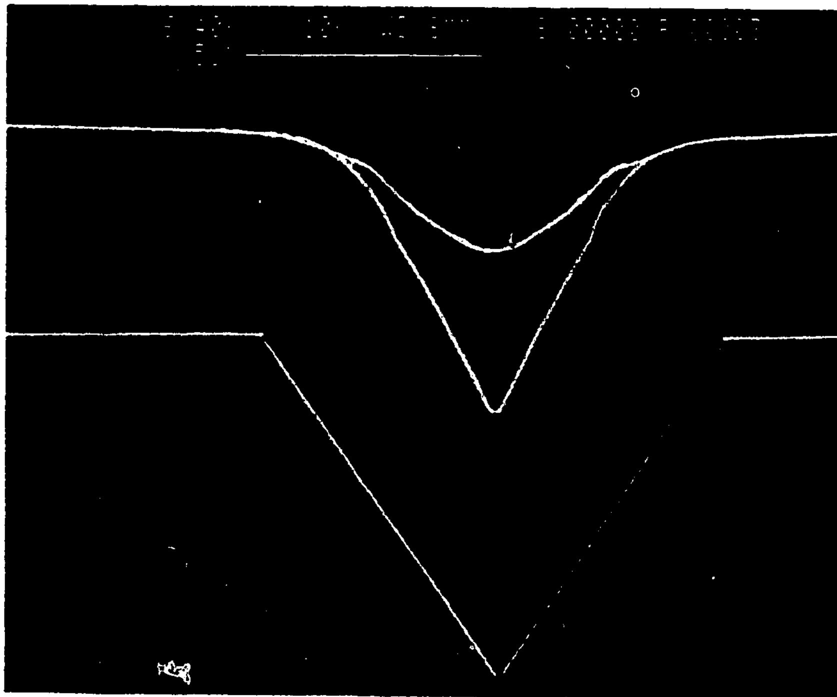

*(d) Silicon V-groove with 3.8 mm silicon dioxide, 2.5 mm * 2.5 mm phosphosilicate glass core after 60 minutes BOE 10:1 etch.*

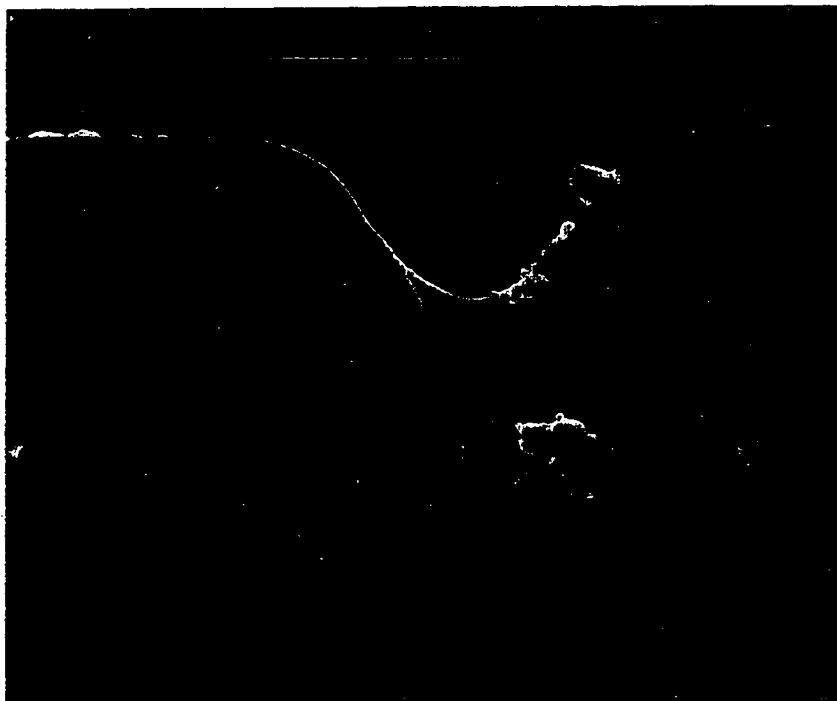

*(e) Silicon V-groove with 3.7 mm silicon dioxide, 2 mm * 2 mm phosphosilicate glass core after 65 minutes BOE 10:1 etch.*

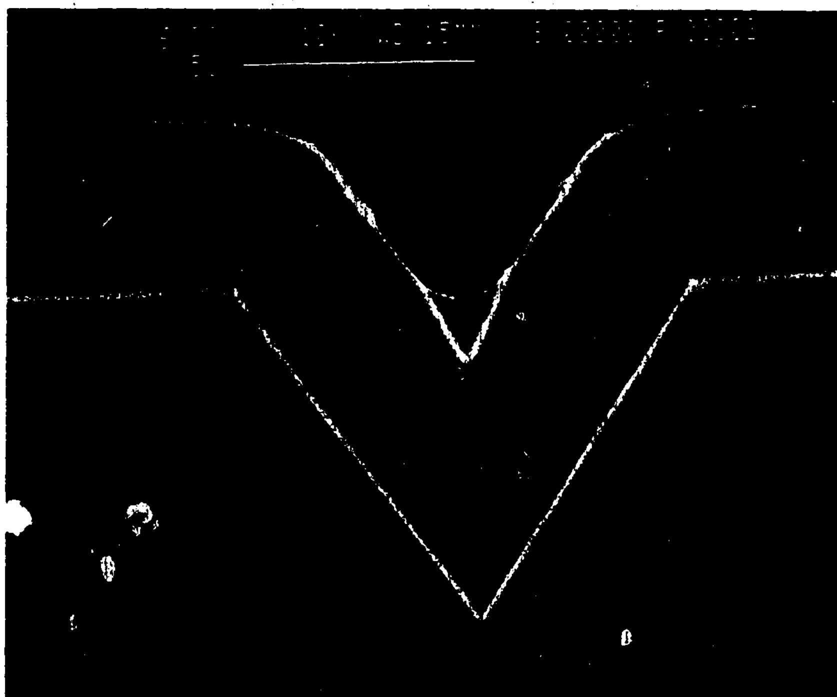

*(f) Silicon V-groove with 3.3 mm silicon dioxide, 1.3 mm * 1.0 mm phosphosilicate glass core after 70 minutes BOE 10:1 etch.*

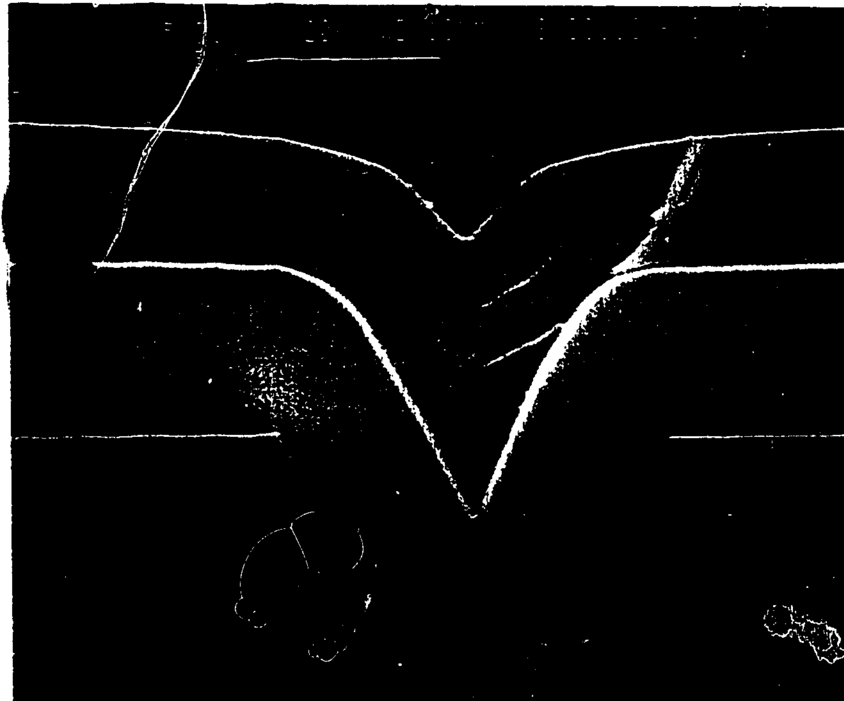

Figure 4.5 (a) Silicon V-groove with 4.5 mm silicon dioxide, 2.5 mm phosphosilicate glass and 3.0 mm silicon dioxide.

Figure 4.5 (b) Silicon V-groove with 4.5 mm silicon dioxide, 2.5 mm phosphosilicate glass and 4.0 mm spin-on-glass.

(vi) Deposition of the cladding layer:

The etch-back is done until the required geometry of the core is obtained. Then a cladding layer is deposited on the core. A cladding layer of CVD silicon dioxide was deposited as shown in the Figure 4.5 (a). The phosphorus-doped oxide core is isolated and prevents coupling of the light between the waveguide grooves. Also spin-on-glass (SOG) was tried as the cladding layer, shown in Figure 4.5 (b). Spin-on-glass needs a high temperature anneal to give a dense, good quality film. The SOG film used was Silica 10,000 which had a refractive index of 1.45. Since the CVD film was adequate for the fabrication process, not much time was spent on the characterization of spin-on-glass.

(vii) Deposition of the metal film for taps:

Deposition of a metal film is necessary to tap light from the waveguide since the silicon-glass interface has only a 16% reflectivity. A metal film which could withstand the CVD process and high temperature annealing without loosing its reflectivity is needed at the end facets to reflect the incident light. A few metal films were deposited, and examined for their reflectivity and surface properties. Different metal films were deposited using vacuum deposition techniques. Silver, chrome-gold and aluminum films were deposited using the thermal evaporator. Molybdenum, chrome, copper and aluminum films were deposited using the electron-beam evaporator. Titanium and aluminum films were sputtered. Reflectivity measurements at normal incidence were done for the wavelength range 600-1550 nm using the spectrophotometer. A 2 μm layer of silicon dioxide was deposited at 450°C using the chemical vapor deposition (CVD) technique and reflectivity measurements were repeated.

Aluminum is the metal film most commonly used with the CVD process and it is the highest reflective film available even after a layer of oxide is deposited. But annealing at 1050°C would destroy the aluminum film as its melting point is only around 660°C. Titanium seems to be the best metal available where annealing of the film is considered a must to provide a dense oxide film. Though the reflectivity is only around 51-67% at normal incidence from visible to infrared wavelengths, it can withstand both the CVD and high temperature annealing and still reflect the same amount of light as it did as a pure metal film. All the other metal films could not be used due to their drawbacks discussed in the Appendix 3.

4.3 LOSS MEASUREMENT:

A 10 mW Helium-Neon laser with a beam diameter of 1 mm and operating at a wavelength of 0.6328 µm is used as the source. The chopper, with a frequency of 200 Hz, is placed in front of the laser and is linked to the lock-in amplifier. Coupling between the laser and single-mode fiber is achieved by focusing the laser beam into the core of the fiber by means of a Newport M-20x microscope objective lens. The single-mode fiber used is Corning Flexor-850 whose mode field diameter is estimated to be 4-6 µm and has a cut-off wavelength of approximately 0.750 µm. Maximum power is coupled into the fiber by precisely adjusting the differential micropositioner on which the fiber is mounted. The fiber in turn couples the light into the trench waveguide with the help of piezoelectric positioners. A plastic fiber with NA of 0.5 is mounted on a micropositioner and collects the scattered light as it travels along the guide. The fiber is connected to the silicon photodetector which is in turn connected to the lock-in amplifier. The loss measurement set-up is shown in the Figure 4.6.

The laser light is launched into the waveguide directly from the end of a single-mode fiber. The end of the wafer upon which the light is shone is cleaved and polished to decrease the amount of light lost due to the edge roughness. The single-mode fiber is butt-coupled to the channel waveguide input end. It is important that the fiber core be aligned accurately both horizontally and vertically with respect to the core of the waveguide. The direct measurement of the propagation loss in the channel waveguides are made by collecting the out-scattered light at right angles to the film using a plastic fiber brought into proximity with the waveguide surface. The fiber is tracked across the waveguide at points along its length and the intensity data for each scan is collected. The logarithm of the transmitted intensity of light is plotted in dB as a function of position. A straight line least squares curve fitting is carried out and the slope gives the loss value. The loss measurements are carried out for many waveguide samples. The loss recorded as shown in Figure 4.7 is 0.1 dB/cm for most of the samples measured. The loss data are attached in Appendix 4. The total insertion loss is 11 dB. It is believed that the high insertion loss is either due to poor coupling, which was not optimized, or radiation into the substrate. The radiation into the substrate can be reduced by increasing the buffer layer thickness or increasing the core doping to more tightly confine the mode.

4.4 NEAR-FIELD INTENSITY MEASUREMENT:

The apparatus to image the waveguide mode was as shown in the Figure 4.8. Light is coupled from a He-Ne laser into the single-mode fiber (Corning Flexor-850)

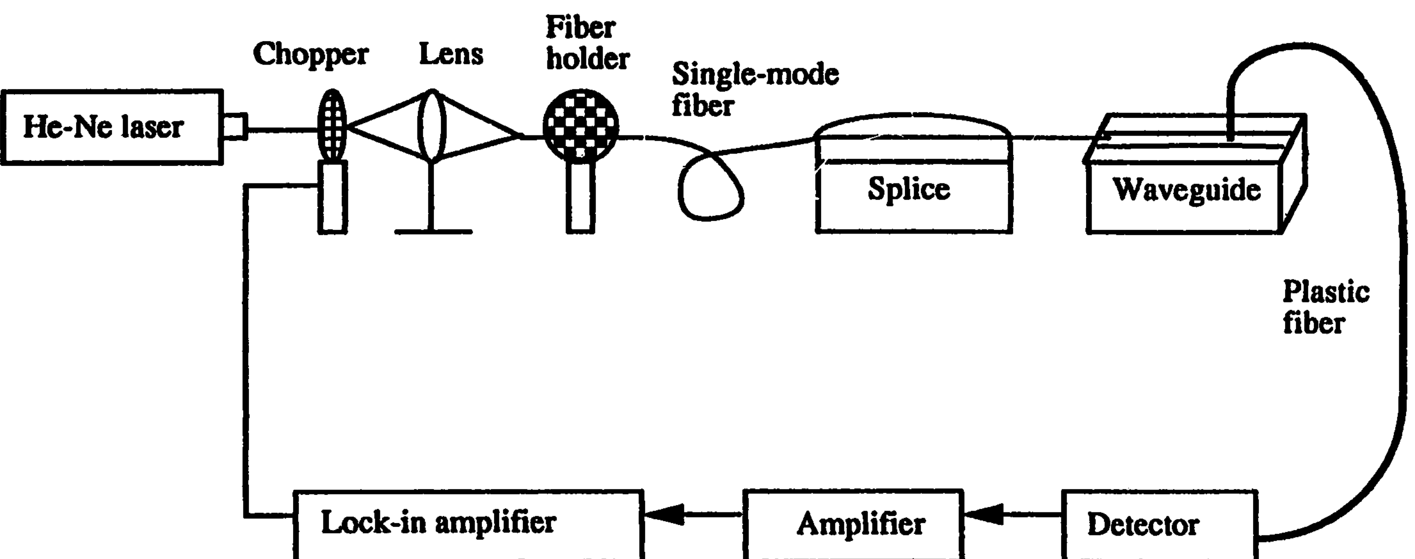

Figure 4.6 Set-up for measuring the channel waveguide scattering losses

PHOSPHORUS-DOPED GLASS CHANNEL WAVEGUIDE-1

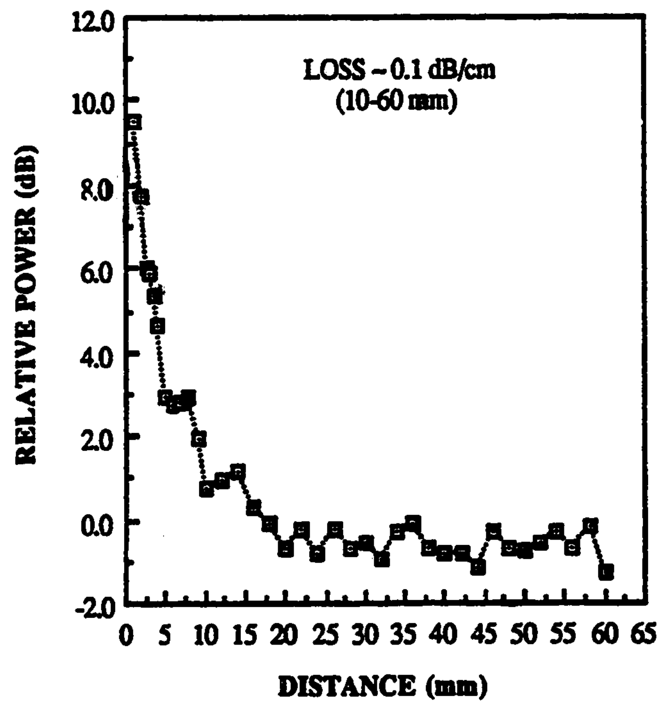

PHOSPHORUS-DOPED GLASS CHANNEL WAVEGUIDE-2

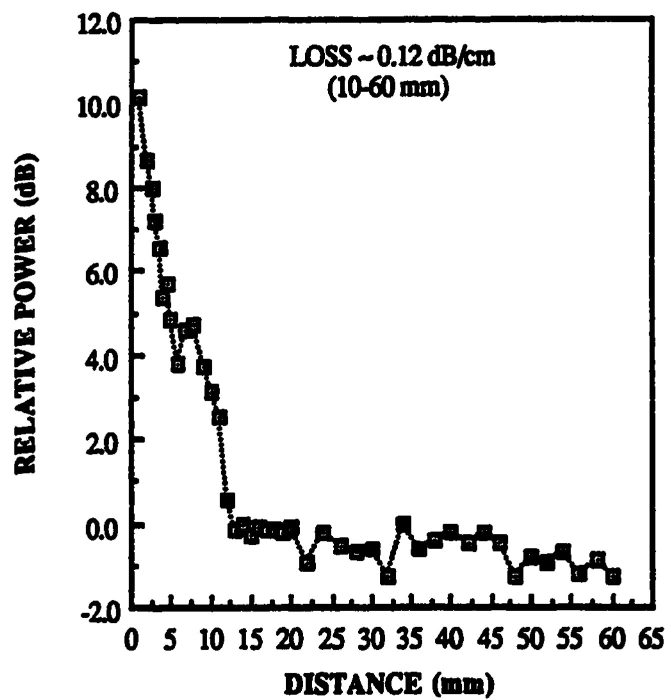

Figure 4.7 Attenuation plots of phosphorus-doped glass channel waveguides.

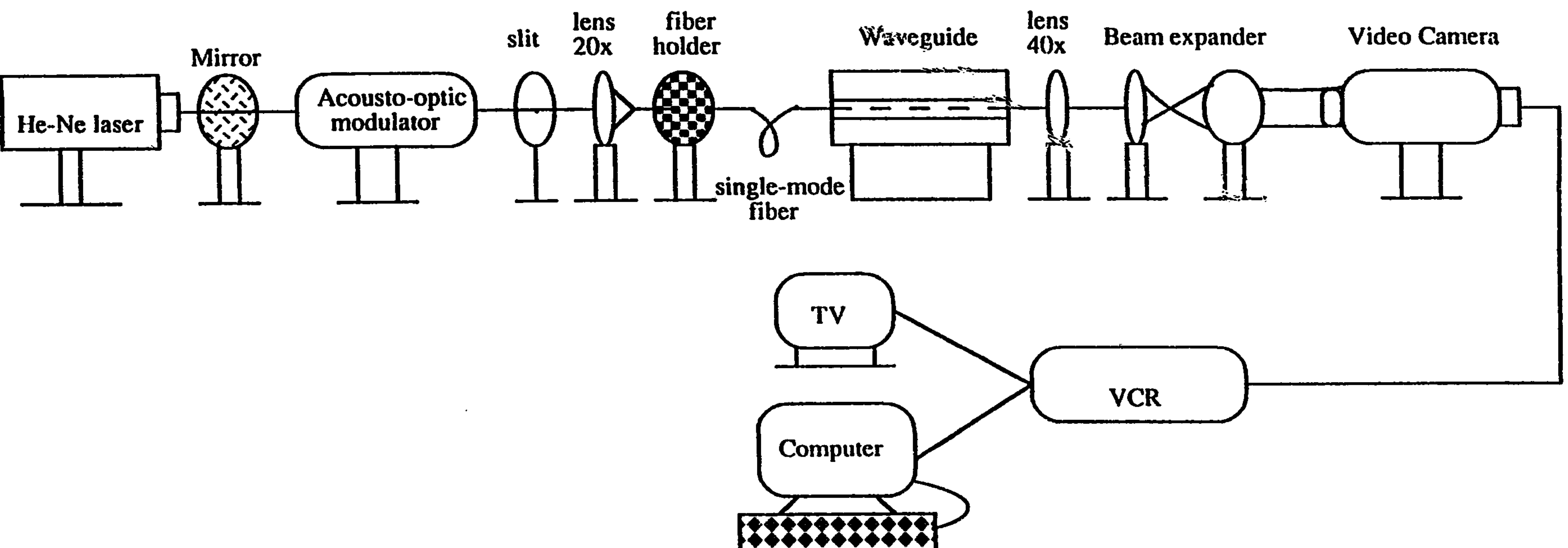

Figure 4.8 Schematic of the near-field intensity measurement.

with the help of a Newport M-20X microscope objective lens. The light from the laser is acousto-optically modulated so that the intensity of the light beam entering the fiber may be controlled. This gives us absolute control of the amount of light entering the video camera. The single-mode fiber is in turn aligned with the cleaved input end of the channel waveguide. Maximum power is coupled into the waveguide with the help of the piezoelectric positioners.

The output mode is observed by imaging the output waveguide facet on a video camera after magnification through a Newport M-40X lens and a beam expander. The output from the video camera is fed into the computer and also fed into the television through a VCR. The output mode is captured with the help of IP Lab software on a Macintosh. The output mode and its contour plot is as shown in the Figure 4.9. The intensity linear plot and the 3-D plot of the output mode is as shown in the Figure 4.10. The mode field shape is gaussian-like. The mode field radius is the beam radius at $1/e^2$ of the maximum power. The mode field diameter, being twice the mode field radius is 7.4 μm for the nabla waveguide. The horizontal and vertical intensity scan of the output mode profile of the phosphorus-doped glass channel waveguide is as shown in the Figure 4.11. The data sheets are attached in the Appendix 4.

The near-field intensity measurement was also tried for higher wavelengths such as 0.880 μm and 0.950 μm using the Titanium-Sapphire laser and Argon laser. It was very difficult to couple a sufficient amount of light to observe the mode. It is believed that this was due to absorption of the mode by the silicon substrate. For the He-Ne wavelength, the buffer layer was thick enough for the light to propagate without being absorbed. To use these waveguides at higher wavelengths, for which the mode size will be bigger, detailed redesigning will be necessary. This can be achieved by increasing the phosphorus concentration and thus increasing the refractive index difference between the core and surrounding layers.

Theoretical designs of the mode profile for the nabla waveguides were done at the University of Waterloo [60] and National Research Council [61]. The theoretical mode profiles are shown in the Figure 4.12. There is a discrepancy between the theoretical and measured profile in that the predicted mode is more tightly bound than the measured mode. Two possible explanations for this inconsistency are:
(a) the refractive index value of the doped and undoped glass is not accurately known,
(b) the image of the measured mode profile has not been focused properly. The resolution of this problem is necessary if nabla waveguides are to be accurately designed.

Simulated propagation of circular beams launched from optical fibers into a nabla waveguide was also done at the University of Waterloo. The beam intensities after 1.6 mm propagation are shown in the Figure 4.13. At 0.633 μm, virtually no power is in the lower cladding. However, at 1.3 μm, dark streaks in the substrate indicate leakage from the core as expected. This may explain our measurement of no transmission at higher wavelengths.

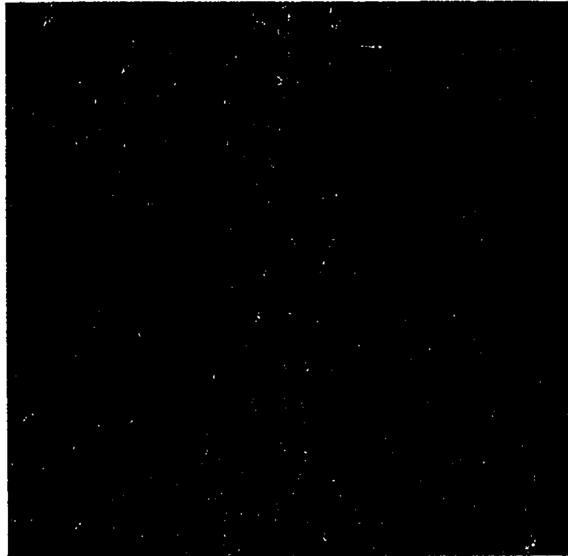

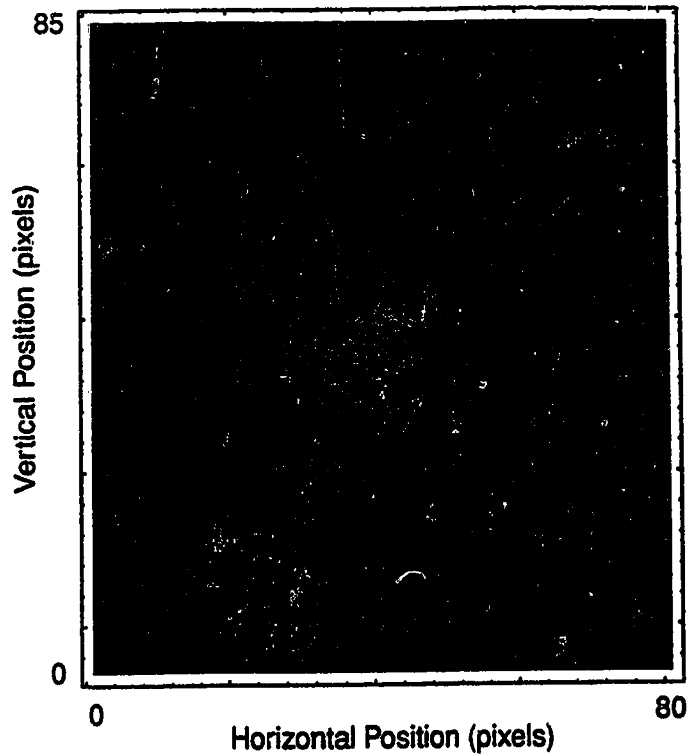

Figure 4.9 Image and the contour plot of the output mode of the single-mode channel waveguide.
1 pixel = 0.132 μm.

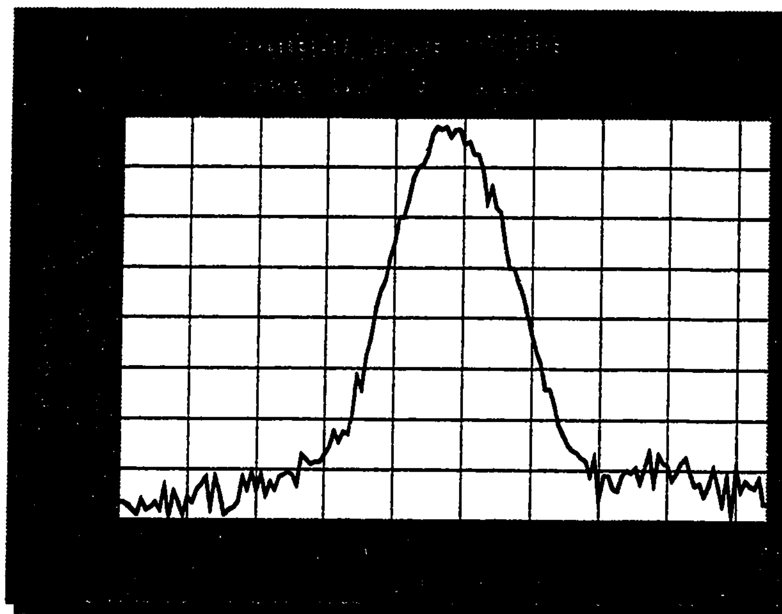

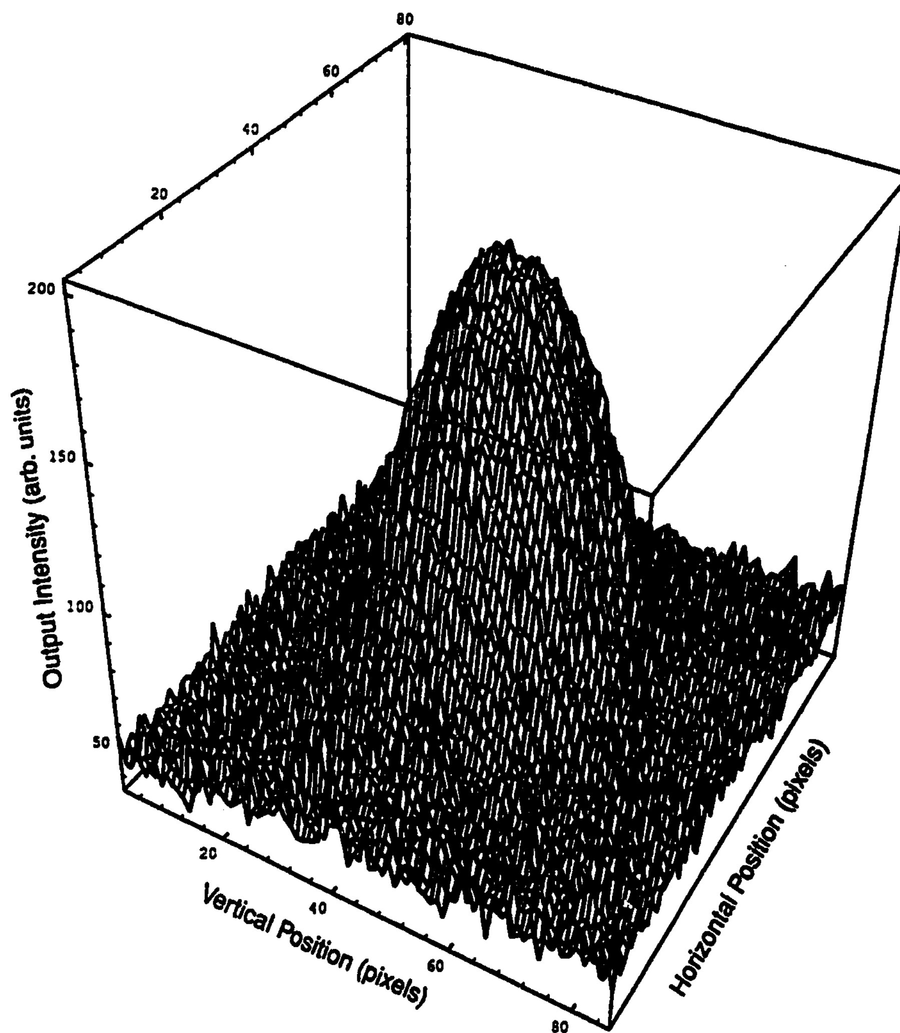

Figure 4.10 Output mode linear and 3-D profile.
1 pixel = 0.132 μm.

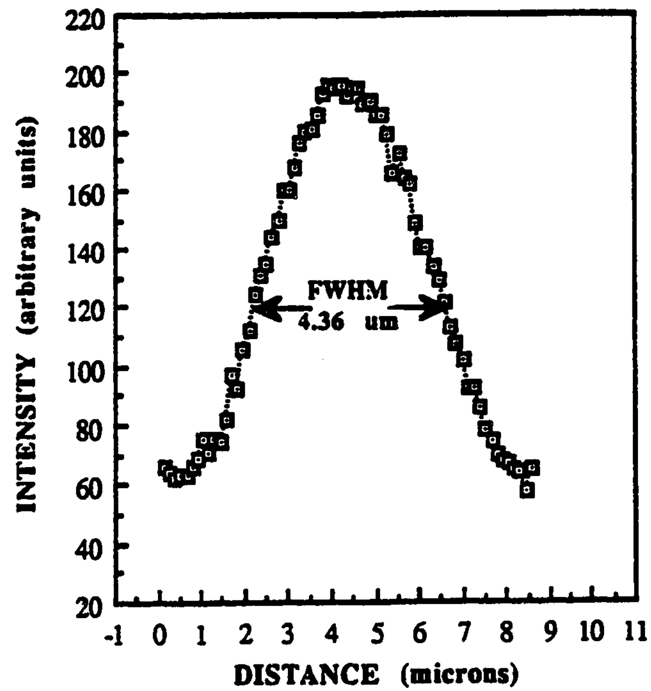

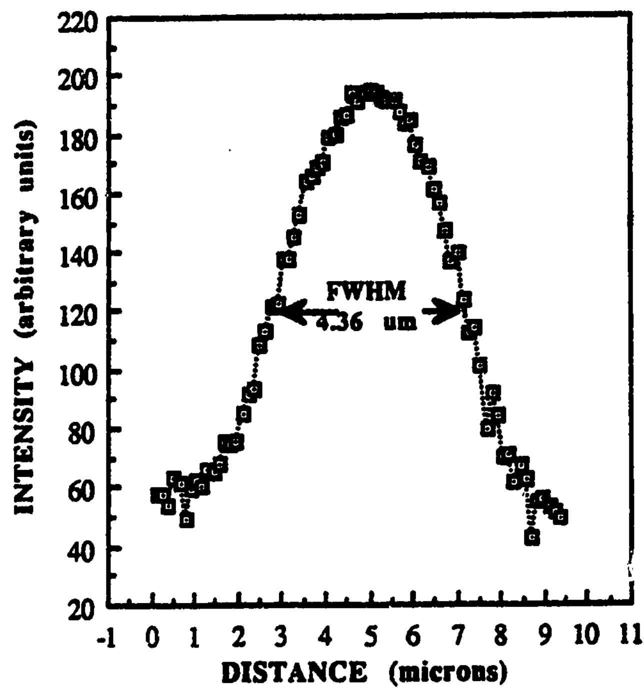

Figure 4.11 Horizontal and vertical scan of the output mode profile.

(a) λ=0.633μm; β=14.723668 λ=1.300μm; β=7.11986931

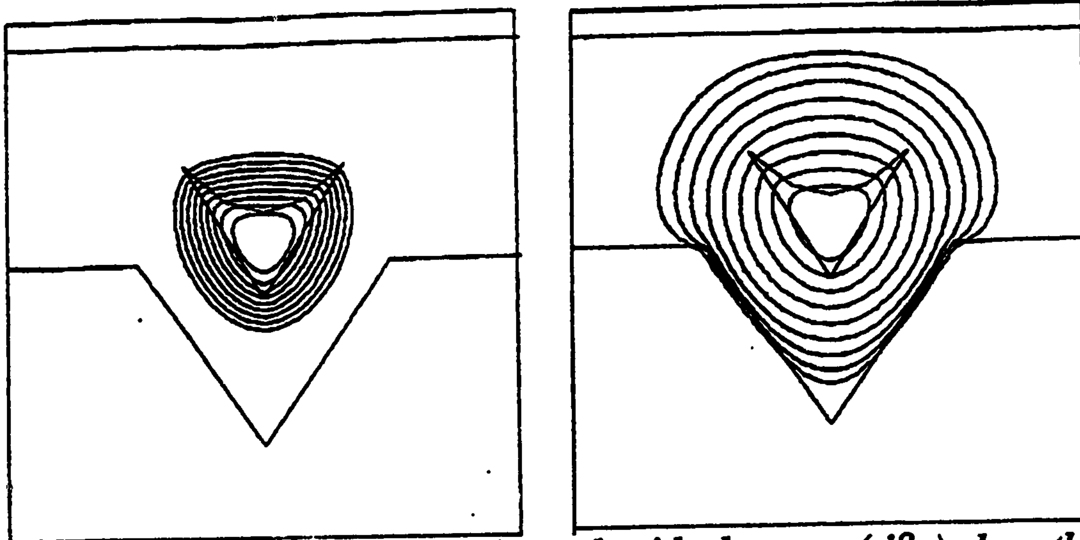

β is the propagation constant for the mode with phase exp (-jβ z) along the waveguide and λ is the operating wavelength.

(b) FIELD INTENSITY (ALL DISTANCES IN μm)

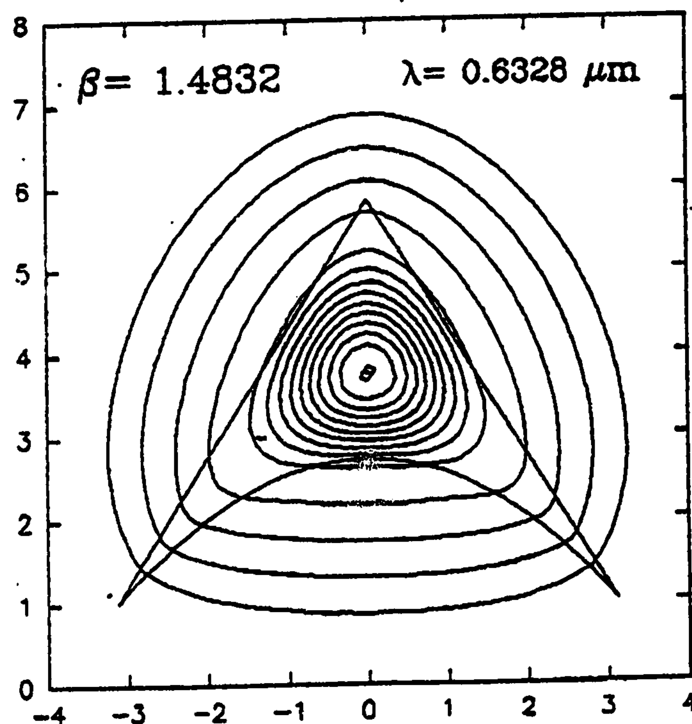

Figure 4.12 Theoretical mode profiles
(a) Predicted mode shape @ 0.633 μm and 1.3 μm (University of Waterloo)
(b) Predicted mode shape @ 0.633 μm (National Research Council)

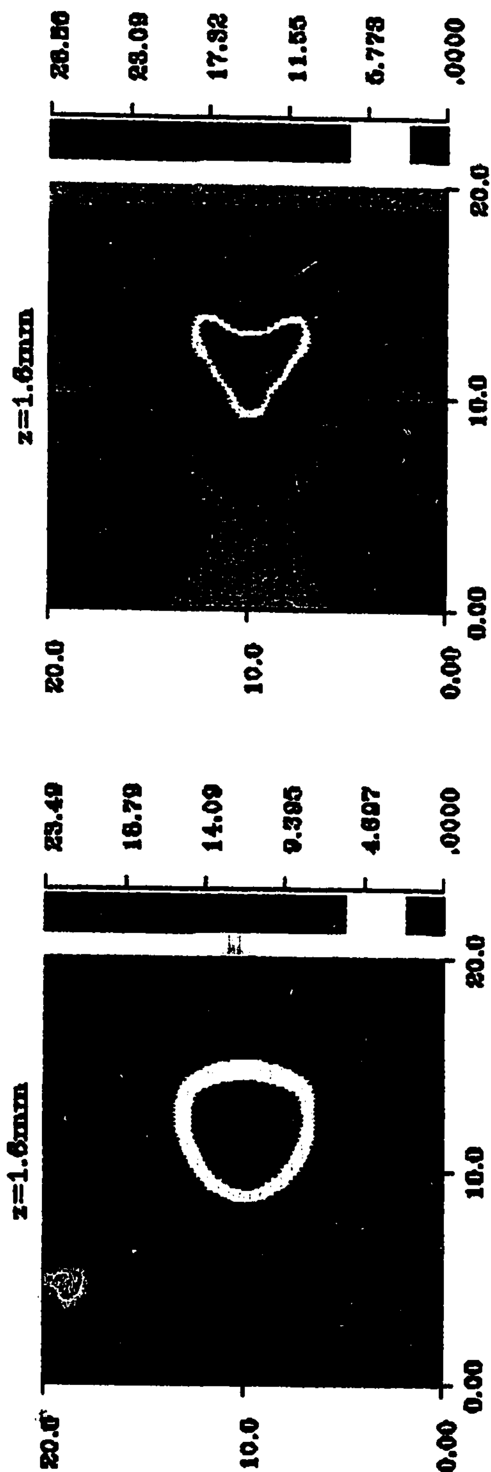

Figure 4.13 Beam profile in waveguide after 1.6 mm of propagation of an optical fiber input beam.
(The dark regions in the substrate at 1.3 μm indicate radiation into the substrate)

5. CONCLUSIONS

In this thesis, the fabrication of phosphorus-doped glass slab and channel waveguides on silicon substrates has been investigated. The waveguiding layers were deposited using low-pressure chemical vapor deposition processes. The slab waveguides provide a simple approach to test the design and fabrication procedure. The slab waveguides have potential use in semi-free-space optical interconnects The channel waveguides have the potential for doped active devices such as lasers and optical amplifiers.

Single-mode, phosphorus-doped glass slab waveguides with step index profiles have been fabricated. The estimated thickness of the phosphosilicate glass core, silicon dioxide buffer and cladding layers are 1.16 μm, 4.5 μm and 3 μm respectively. The phosphorus-doped glass slab waveguides exhibited a loss of 0.05 dB/cm at 0.6328 μm wavelength. The phosphorus-doped slab waveguides may be used in future in semi-free-space optical interconnect.

Phosphorus-doped glass waveguides in silicon V-grooves have been fabricated. CVD glass waveguides formed in silicon V-grooves involve the difficulty of removing the glass off the areas between the guides. This particular problem was dealt with by filling up the grooves with phosphorus doped glass and then etching back to get the required core shape and thickness. A novel, reproducible fabrication technique for batch processing multichannel single-mode CVD glass channel waveguides is presented. The estimated required thicknesses of the silicon dioxide buffer and cladding layers are 4.5 μm and 3 μm respectively. Approximate design considerations for single-mode propagation in the nabla waveguide indicate core width and depth of 1.88 μm and 1.33 μm respectively.

Scattering loss measurements were carried out and these waveguides exhibited a low propagation loss of 0.1 dB/cm at 0.6328 μm. The output mode of the waveguide was imaged at 0.6328 μm and the mode field diameter was found to be 7.4 μm. There is a discrepancy between the theoretical and measured mode profiles. Two possible explanations for this inconsistency are the refractive index value of the doped and undoped glass is not accurately known and the image of the measured mode profile has not been focused properly. The resolution of this problem is necessary if nabla waveguides are to be accurately designed. At higher wavelengths, the fundamental mode appears to radiate into the silicon substrate. The dark regions in the substrate at 1.3 μm (see Figure 4.12) confirm the radiation into the substrate.

The waveguides need redesigning for higher wavelengths as most of the applications lie in the longer wavelength region.

Alignment grooves can be also be made to fit the fiber in the groove and butt-couple to the glass waveguide deposited in the V-groove. The grooves for both the fiber and the waveguide may need a single masking and etching step. Since the waveguides will be used to achieve better coupling efficiency with the fiber, the mode field shape of the single-mode fiber and single-mode nabla waveguide have to be accurately matched, which can be considered as a separate project. To tightly confine the mode within the core, we must increase the phosphorus doping concentration, which in turn increases the refractive index difference of the core. Also, to prevent any absorption by the silicon substrate, thicker buffer layers are recommended. Accurate theoretical calculations are recommended to predict the mode shape and size.

Out-of-plane coupling is required to use these waveguides in an optical switch. To tap the light out of the end facets of these waveguides, the core must be buried within the silicon V-groove. The tapping of light from the phosphorus-doped glass waveguides were not carried out in this thesis. This will be considered later as a major future project. Also the possibility of tapping the light by using gratings on the core surface may be considered. The nabla waveguides can be used in future to fabricate doped glass active devices such as the lasers (dye lasers) and optical amplifiers (erbium-doped amplifiers).

BIBLIOGRAPHY

(1) **S.E. Miller**, "Integrated optics: an introduction", The Bell System Technical Journal, Vol. 48, No. 7, September 1969, pp. 2059-2069.

(2) **H. Nishihara, M. Haruna and T. Suhara**, "Optical integrated circuits", McGraw-Hill Optical and Electro-Optical Engineering Series, R.E Fisscher and W.J. Smith, Series Editors, 1989.

(3) **C.H. Henry, G.E. Blonder and R.F. Kazarinov**, "Glass waveguides on silicon for hybrid optical packaging", Journal of Lightwave Technology, Vol. 7, No. 10, October 1989, pp. 1530-1539.

(4) **R.M. Levin and A.C. Adams**, "Low-pressure deposition of phosphosilicate glass films", Journal of Electrochemical Society, Vol. 129, No. 7, July 1982, pp.1588-1592.

(5) **C. Dragone, C.H. Henry, I.P. Kaminow and R.C. Kistler**, "Efficient multichannel integrated optics star coupler on silicon", IEEE Photonics Technology Letters, Vol. 1, No. 8, August 1989, pp. 241-243.

(6) **B.H. Verbeek, C.H. Henry, N.A. Olsson, K.J. Orlowsky, R.F. Kazarinov and B.H. Johnston**, "Integrated four-channel Mach-Zehnder multi/demultiplexer fabricated with phosphorus-doped silicon dioxide waveguides on silicon", Journal of Lightwave Technology, Vol. 6, No. 6, June 1988, pp. 1011-1015.

(7) **S. Valette, P. Gidon and J.P. Jadot**, "New integrated optical multiplexer-demultiplexer realized on silicon substrate", Proceedings, Fourth European Conference on Integrated Optics, ECIO 87, Glasgow, May 11-13, 1987, C.D.W. Wilkinson and J. Lamb, Editors, pp. 145-147.

(8) **Y. Shani, C.H. Henry, R.C. Kistler, K.J. Orlowsky and D.A. Ackerman**, "Efficient coupling of a semiconductor laser to an optical fiber by means of a tapered waveguide on silicon", Applied Physics Letters, Vol. 55, No. 23, December 1989, pp. 2389-2391.

(9) **Y. Shani, C.H. Henry, R.C. Kistler, R.F. Kazarinov and K.J. Orlowsky**, "Integrated optic adiabatic polarization splitter on silicon", Applied Physics Letters, Vol. 50, No. 2, January 1990, pp. 120-121.

(10) **A. Naumaan and J.T. Boyd**, "A geodesic optical waveguide lens fabricated by anisotropic etching", Applied Physics Letters, Vol. 35, No. 3, August 1979, pp. 234-236.

(11) **A. Naumaan and J.T. Boyd**, "Ring resonator fabricated in phosphosilicate glass films deposited by chemical vapor deposition", Journal of Lightwave Technology, Vol. 4, No. 9, September 1986, pp. 1294-1303.

(12) **K.E. Petersen**, "Silicon as a mechanical material", Proceedings of the IEEE, Vol. 70, No. 5, May 1982, pp. 420-457.

(13) **E. Bassous**, "Fabrication of novel three-dimensional microstructures by the anisotropic etching of <100> and <110> Silicon", IEEE Transactions on Electron Devices, Vol. 25, No. 10, October 1978, pp. 1178-1185.

(14) **K.E. Bean**, "Anisotropic etching of silicon", IEEE Transactions on Electron Devices, Vol. 25, No. 10, October 1978, pp. 1185-1193.

(15) **J.T. Boyd and S. Sriram**, "Optical coupling from fibers to channel waveguides formed on silicon", Applied Optics, Vol.17, No. 6, March 1978, pp. 895-898.

(16) **S.K. Chen and J.N. McMullin**, "A $1x2^m$ integrated star coupler using diffraction gratings", Proceedings of the 2nd IEEE International Workshop on Photonic Networks, Components and Applications, Monte Bello, Canada, 9-11 March, 1992 (OCRI Publications, Kanata, Canada).

(17) **N. Takato, K. Jinguji, M. Yasu, H. Toba and M. Kawachi**, "Silica-based single-mode waveguides on silicon and their application to guided-wave optical interferometers", Journal of Lightwave Technology, Vol. 6, No. 6, June 1988, pp. 1003-1010.

(18) **R.R. Krchnavek, G.R. Lalk and D.H. Hartman**, "Laser direct writing of channel waveguides using spin-on polymers", Journal of Applied Physics, Vol. 66, No. 11, Dec 1989, pp. 5156-5160.

(19) **S. Dutta, H.E. Jackson, J.T. Boyd, R.L.Davis and F.S. Hickernell**, "CO_2 laser annealing of Si_3N_4, Nb_2O_5 and Ta_2O_5 thin-film optical waveguides to achieve scattering loss reduction", IEEE Journal of Quantum Electronics, Vol. 18, No. 4, April 1982, pp. 800-806.

(20) **W. Stutius and W. Streifer**, " Silicon nitride films on silicon for optical waveguides ", Applied Optics, Vol. 16, No. 12, December 1977, pp. 3218-3222

(21) **S. Dutta, H.E. Jackson, J.T. Boyd, F.S. Hickernell and R.L.Davis**, "Scattering loss reduction in ZnO optical waveguides by laser annealing", Applied Physics Letters, Vol. 39, No. 3, August 1981, pp. 206-208.

(22) **S. Dutta, H.E Jackson and J.T. Boyd**, "Extremely low-loss glass thin-film optical waveguides utilizing surface coating and laser annealing", Journal of Applied Physics, Vol. 52, No. 6, June 1981, pp. 3873-3875.

(23) **D.E. Zelmon, H.E. Jackson, J.T. Boyd, A. Naumaan and D.B. Anderson**, "A low scattering graded-index silicon dioxide planar optical waveguide Thermally grown on Silicon", Applied Physics Letters, Vol. 42, No. 7, April 1983, pp. 565-566.

(24) **A. Naumaan and J.T. Boyd**, " Laser annealing of phosphosilicate glass, Journal of Vacuum Science Technology, Vol. 18, No. 3, April 1981, pp. 821-824.

(25) **F.S. Hickernell**, "Optical waveguides on silicon", Solid state technology, November 1988, pp. 83-88.

(26) **E.A. Taft**, "The optical constants of Silicon and dry oxygen oxides of silicon at 5461 Å", Journal of Electrochemical Society, Vol. 125, No. 6, 1978, pp. 968-971.

(27) **D.E. Zelmon, J.T. Boyd and H.E. Jackson**, "Low-loss optical waveguides fabricated by thermal nitridation of oxidized silicon", Applied Physics Letters, Vol. 47, No. 4, August 1985, pp. 353-355.

(28) **M.J. Rand and R.D. Stanley**, "Silicon oxynitride films on fused silica for optical waveguides", Applied Optics, Vol. 11, No. 11, November 1972, pp. 2482-2488.

(29) **M. Kawachi, M. Yasu and M. Kobayashi**, "Flame hydrolysis deposition of SiO_2 and TiO_2 glass planar optical waveguides on silicon", Japanese Journal of Applied Physics, Vol. 22, No. 12, 1983, p. 1932.

(30) **M.A. Duguay, J.Y. Kokubun, T.L. Koch and L. Peiffer**, "Antiresonant reflecting optical waveguides in SiO_2-Si multilayer structures", Applied Physics Letters, Vol. 49, No.1, July 1986, pp. 13-15.

(31) **I.K. Naik**, "Low-loss integrated optical waveguides fabricated by Nitrogen ion implantation", Applied Physics Letters, Vol. 43, No. 6, September 1983, pp. 519-520.

(32) **W.S.C. Chang, M.W. Muller and F.J. Rosenbaum**, "Integrated optics", Laser Applications, Vol. 2, M. Ross, Editor, Academic Press, New York, 1974.

(33) **F.S. Hickernell, F.Y. Cho, F.V. Richard and T.S. Hickernell**, "Zinc oxide channel waveguide formation on etched ridge structures", Proc. IEEE Ultrasonic Symposium, 1983, p. 353.

(34) **T. Izawa, H. Mori, Y. Murakami and N. Shimizu**, "Deposited silica waveguide for integrated optical circuits", Applied Physics Letters, Vol. 38, No. 7, April 1981, pp. 483-485.

(35) **J.T. Boyd, R.W. Wu, D.E. Zelmon, A. Naumaan, H.A. Timlin and H.E. Jackson**, "Guided wave optical structures utilizing silicon", Optical Engineering, Vol. 24, No. 2, March/April 1985, pp. 230-234.

(36) **C.H. Henry, R.F. Kazarinov, H.J. Lee, K.J. Orlowsky and L.E. Katz**, "Low-loss Si_3N_4-SiO_2 optical waveguides on silicon", Applied Optics, Vol. 26, No. 13, July 1987, pp. 2621-2624.

(37) **S. Valette, J.P. Jadot, P. Gidon, S. Renard, A. Fournier, A.M. Grouillet, H. Denis, P. Philippe and E. Desgranges**, "Silicon-based integrated optics technologies", Solid State Technology, February 1989, pp. 69-74.

(38) **S. Valette**, "State of the art of integrated optics technology at LETI for achieving passive optical component, Journal of Modern Optics, Vol. 35, No. 6, 1988, pp. 993-1005.

(39) **N. Takato, M. Yasu and M. Kawachi**, "Low-loss high-silica single-mode channel waveguides", Electronics Letters, Vol. 22, March 1986, pp. 321-322.

(40) **J.S. Harper and P.H. Heidrich**, "High density multichannel optical waveguides with integrated couplers", Wave Electronics, Vol. 2, 1976, pp. 369-377.

(41) **W.T. Tsang, C.C. Tseng and S. Wang**, "Optical waveguides fabricated by preferential etching", Applied Optics, Vol. 14, No. 5, May 1975, pp. 1200-1206.

(42) **C.C. Tseng, D. Botez and S. Wang**, "Optical bends and rings fabricated by preferential etching", Applied Physics Letters, Vol. 26, No. 12, June 1975, pp. 699-701.

(43) **S.L. Chen and J.T. Boyd**, "Integrated optical beam splitters formed in glass channel waveguides having variable weighting as determined by mask dimensions", IEEE Journal of Quantum Electronics, Vol. 18, No. 7, July 1982, pp. 1072-1077.

(44) **S. Kumar, R.I. MacDonald and J.N. McMullin**, "Low-loss multimode polymer waveguides with serial out-of-plane taps", Digest of Conference on Optical Fiber Communication, 1992 OSA Technical Digest Series, Vol. 5 (Optical Society of America, Washington, D.C., 1992), p. 267.

(45) **L.P. Boivin**, "Thin-film laser-to-fiber coupler", Applied Optics, Vol. 13, No. 2, February 1974, pp. 391-395.

(46) **R.M. Cline**, "Investigating the characteristics of doped-glass waveguides on silicon substrates", Co-op work term report, TR Labs, Edmonton, August 1990.

(47) **C.P. Ho, S.E. Hansen and P.M. Fahey**, "Suprem III, a program for integrated circuit process modeling and simulation", Technical Report No. SEL 84-001, Stanford University, CA, USA, 1984.

(48) **G.L. Schnable, W. Keen and R.B. Comizzoli**, "Passivation coatings on silicon devices", Journal of Electrochemical Society, Vol. 122, No. 8, August 1975, pp. 1092-1103.

(49) **M.M. Schlacter, E.S. Schlegel, R.S. Keen, Jr. R.A. Lathlaen and G.L. Schnable**, "Advantages of vapor-plated phosphosilicate films in large-scale integrated circuit arrays", IEEE Transactions on Electron Devices, December 1970, pp. 1077-1083.

(50) **J.B. Angell, S.C. Terry and P.W. Barth**, "Silicon micromechanical devices", Science America, April 1983, pp. 36-47.

(51) **E. Bassous**, U.S. Patent 3,921,916, (1975).

(52) **A. Naumaan and J.T. Boyd**, "Phosphosilicate glass flow for integrated optics", Journal of Vacuum Science and Technology, Vol. 17, No. 1, January/February 1980, pp. 529-532.

(53) **S. Valette, J. Lizet, P. Mottier, J.P. Jadot, P. Gidon and S. Renard**, "Integrated-optical circuits achieved by planar technology on silicon substrates: application to the optical spectrum analyser", IEEE proceedings, Part H, Vol. 131, No. 5, October 1984, pp. 325-331.

(54) **A.C. Adams, C. D. Capio, S.E. Haszko, G.I. Parisi, E.I. Povilonis and McD. Robinson**, "The high temperature deposition and evaluation of phosphorus- or boron-doped silicon dioxide films", Journal of Electrochemical Society, Vol. 126, No. 2, February 1979, pp. 313-319.

(55) **H.J. Lee, C.H. Henry, K.J. Orlowsky, R.F. Kazarinov and T.Y. Kometani**, "Refractive-index dispersion of phosphosilicate glass, thermal oxide and silicon nitride films on silicon", Applied Optics, Vol. 27, No. 19, October 1988, pp. 4104-4109.

(56) **A.C. Adams and S.P. Murarka**, "Measuring the phosphorus concentration in deposited phosphosilicate films", Journal of Electrochemical Society, Vol. 126, No. 2, February 1979, pp. 334-338.

(57) **W.E. Armstrong and D.L. Tolliver**, "A scanning electron microscope investigation of glass flow in MOS integrated circuit fabrication", Journal of Electrochemical Society, Vol. 126, No. 2, February 1974, pp. 307-310.

(58) **G. McKinnon and Y. Loke**, "Silicon micromachining", Course notes, Alberta Microelectronic Centre, Edmonton, February 1991.

(59) **K. Imoto, H. Sano and M. Miyazaki**, "Guided-wave multi/demultiplexers with high stopband rejection", Applied Optics, Vol. 26, No. 19, October 1987, pp. 4214-4219.

(60) **W. Huang and S. Chaudhari**, Department of Electrical Engineering, University of Waterloo, Private Communication.

(61) **A. Delage**, National Research Council, Ottawa, Private Communication.

(62) **D.J. Elliott**, "Microlithography: process technology for IC fabrication", McGraw-Hill Book Company, New York, 1986.

(63) **D.J. Elliott**, "Integrated circuit fabrication technology", II edition, McGraw-Hill Publishing Company, New Jersey, 1989.

(64) **P. Gise and R. Blanchard**, "Modern semiconductor fabrication technology", Prentice-Hall Publishing Company, New Jersey, 1986.

APPENDIX 1

A.1.1 DESIGN OF SLAB WAVEGUIDE [2]:

The single mode slab waveguide has a step index of refraction as shown in the Figure A.1.1.

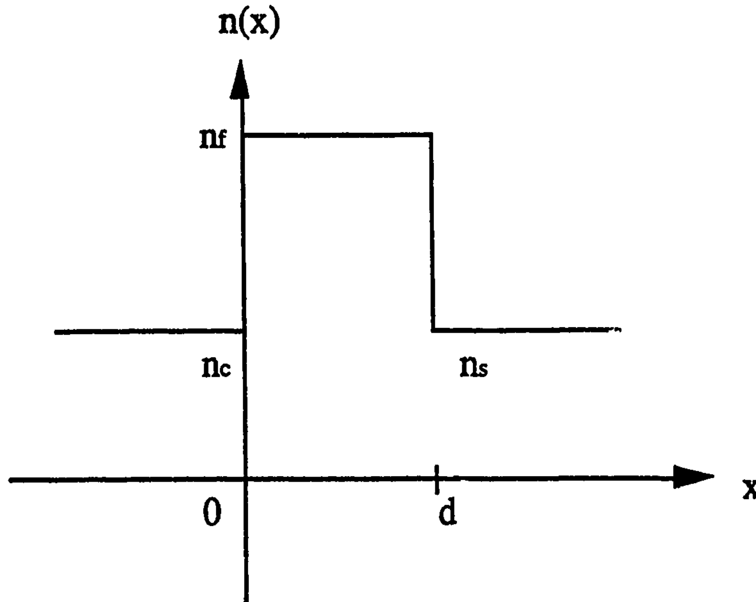

Figure A.1.1 Step index profile

where n_s = substrate index = 1.46 (pure silicon dioxide)

n_f = guiding film index = 1.485 (10 wt. % phosphorus doped glass)

n_c = cladding index = 1.46 (pure silicon dioxide)

The normalized frequency is given by

$$V = k_0 d \sqrt{n_f^2 - n_s^2}.$$

where

$$k_0 = \frac{2\pi}{\lambda}$$

A possible range of the normalized frequency is determined so that the fundamental mode with mode number m=0 is guided while the first-order mode with m=1 is cut off. The range of V selected to meet the single mode requirement is

$$\tan^{-1}\sqrt{a} < V \leq \pi + \tan^{-1}\sqrt{a}.$$

For symmetrical waveguides $n_s = n_c$, a=0, where a is the waveguide asymmetry parameter, therefore,

$$0 < V \leq \pi.$$

This implies that the fundamental mode is not cut off in a symmetrical waveguide.

Therefore

$$V < \frac{2\pi}{\lambda} d \sqrt{n_f^2 - n_s^2} \leq \pi .$$

and solving for d, the thickness of the guiding film

$$d \leq \frac{\lambda}{2\sqrt{n_f^2 - n_s^2}} .$$

For a singlemode slab waveguide at He-Ne wavelength of 0.6328 μm, the required film thickness is found to be 1.16 μm. For a guiding film thickness of 1.0 μm the minimum buffer layer thickness required is 4.5 μm as shown in the Figure A.2.2. The cladding layer is 3.0 μm thick.

A.1.2 : SUPREM III DIFFUSION PROCESS MODELING:

The diffusion of phosphorus into the oxide was characterized using the SUPREM III, a program for integrated circuit process modeling and simulation developed at Stanford University [47]. The diffusion of 10 wt. % phosphorus in silicon dioxide was found under these conditions: 120 minutes anneal at 1000°C in the nitrogen ambient with the diffusivity constant of 7.6×10^{-3} cm^2/sec. The phosphorus concentration in atoms/cm^3 is calculated as follows:

Concentration of silicon dioxide 'x' = 2.2×10^{22} cm^{-3}

Multiply by (weight of silicon dioxide 'w_1' = 60.08)

Total weight of silicon dioxide 'w_1x' (2.2×10^{22} $cm^{-3} \times 60.08$)

Concentration of phosphorus 'y'

Multiply by (weight of phosphorus 'w_2' = 30.97)

Total weight of phosphorus 'w_2y' (y x 30.97)

$$\% \text{ wt.} = \frac{w_2y}{w_2y + w_1x} .$$

and solving for y,

$y = 4.74 \times 10^{21}$ atoms/cm^3

The diffusion of phosphorus into the silicon dioxide layers is plotted as shown in Figure A.1.2. The junction depth is the thickness of the oxide layers. The phosphorus-doped oxide is between 3 to 4 μm and the silicon dioxide layers are between 1 to 3 μm and 4 to 7 μm. The profile of the index of refraction is STEP which results in an abrupt change of index. There is very little diffusion of 10 wt. % phosphorus into the oxide layers even after a high temperature anneal. The step index profile remains intact.

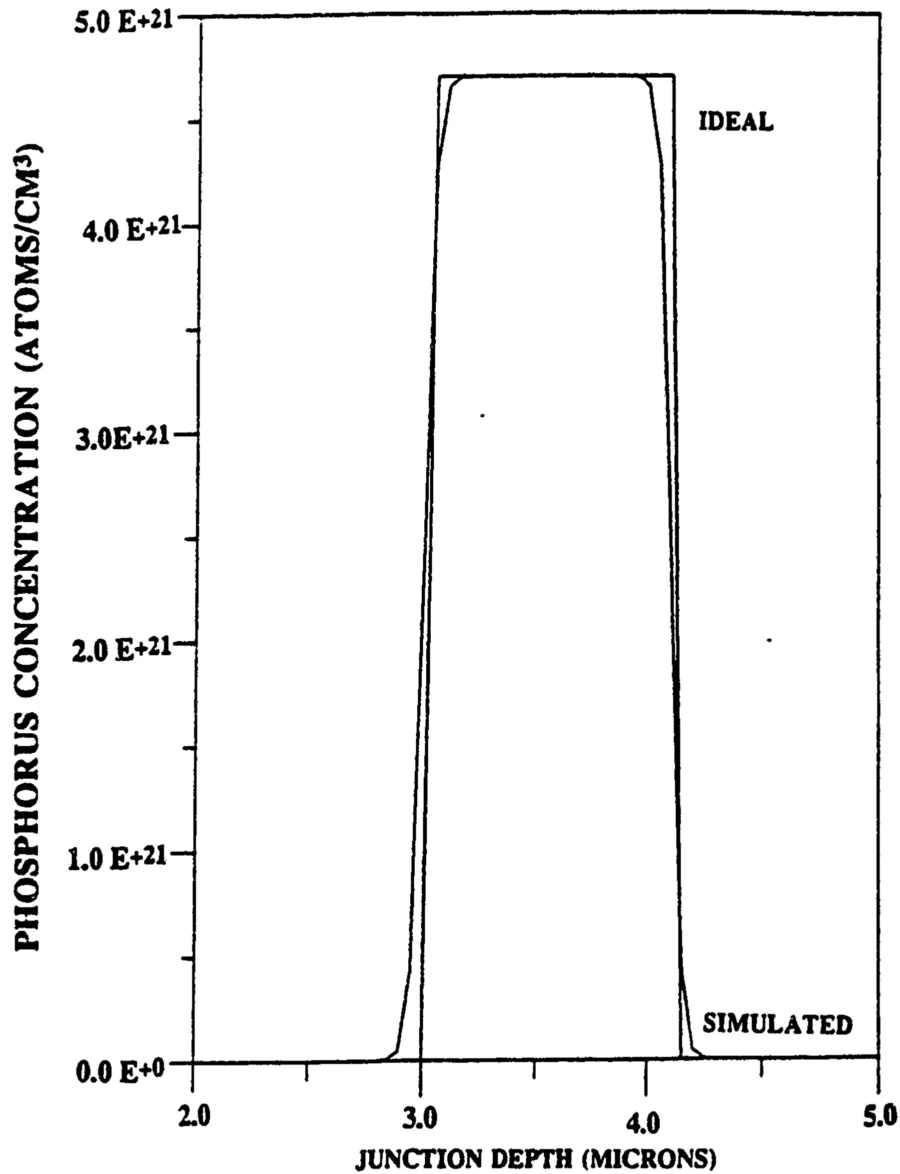

Figure A.1.2 Diffusion of 10 wt.% phosphorus in silicon dioxide using Suprem III process modelling.
Conditions : 120 minutes anneal at 1000°C in nitrogen ambient at diffusivity $D_0 = 7.6 \times 10^{-3}$ cm²/s

APPENDIX 2

A.2.1 DESIGN OF SINGLEMODE CHANNEL WAVEGUIDE:

The area of the triangular waveguide is equated to that of a cylindrical fiber. The geometries of the triangular core waveguide and the cylindrical fiber is as shown in the Figure A.2.1.

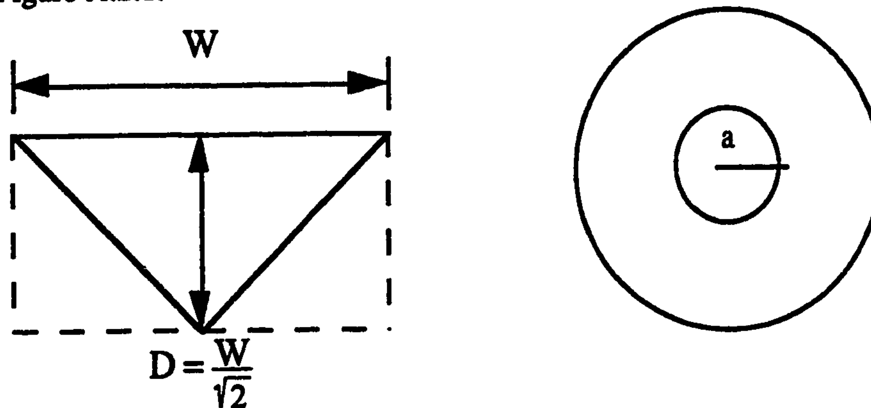

Figure A.2.1 Geometry of the triangular core and cylindrical fiber

The area of the triangular core is

$$A = W \times \frac{W}{\sqrt{2}} = \frac{W^2}{\sqrt{2}}.$$

The condition of single-mode propagation in a circular fibre is

$$V < 2.4$$

where the normalized frequency V is given by

$$V = \frac{2\pi}{\lambda} a \sqrt{n_f^2 - n_s^2}.$$

The area of the circular fibre is

$$A = \pi a^2$$

where,

$$a = \sqrt{\frac{A}{\pi}} = \sqrt{\frac{W^2}{\sqrt{2}\,\pi}} = 0.632\,W.$$

and the normalized frequency,

$$V = \frac{2\pi}{\lambda} \frac{W}{\sqrt{\pi} \times 2^{0.25}} \sqrt{n_f^2 - n_s^2} \leq 2.4.$$

Therefore,

$$W \leq \frac{2.4 \times \lambda \sqrt{\pi} \times 2^{0.25}}{2\,\pi\,(NA)} \leq 0.805 \left\{\frac{\lambda}{NA}\right\}.$$

Here $NA = \sqrt{n_f^2 - n_s^2} = 0.27$ and $\lambda = 0.6328\ \mu m$,

Therefore,

$$W \leq 1.88\ \mu m$$

Since,

$$D \leq \frac{W}{\sqrt{2}} \leq 1.33\ \mu m\,.$$

The core thickness must be 1.3 μm, the minimum buffer thickness must be 4.5 μm as shown in Figure A.2.2 and the cladding layer is 3.0 μm.

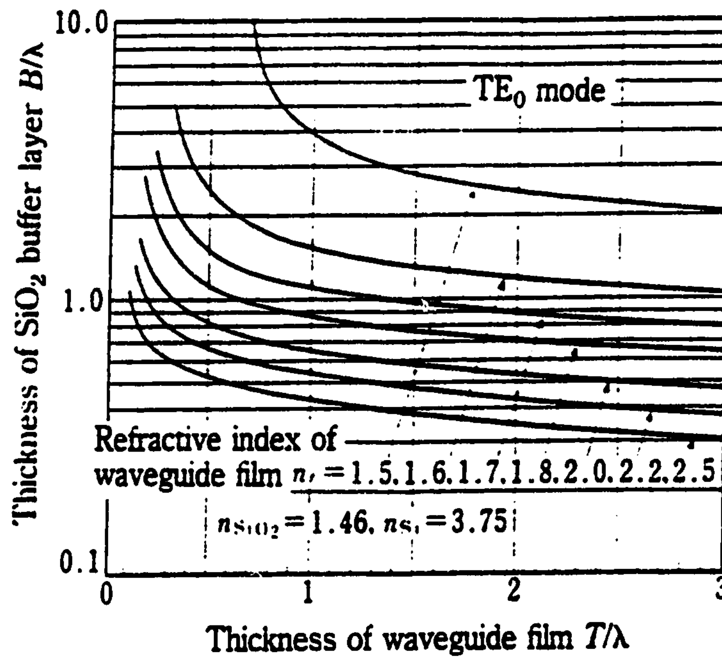

Figure A.2.2 Minimum SiO_2 buffer layer thickness required to reduce the leakage loss of waveguides on SiO_2/Si substrate to 0.1dB/$10^4\lambda$ (~0.1dB/cm).

(Figure A.2.2 is taken from the text Optical Integrated Circuits, H. Nishihara, M. Haruna and T.Suhara, Mcgraw Hill, 1989).

APPENDIX 3

A.3.1 PHOTOLITHGRAPHY RECIPE [58]:

Substrate:

Silicon wafers: <100> orientation, p-type dopant, 1-10 ohm resistivity
98.5-101.2 cm diameter, 457-559 μm thickness.

Thermal oxidation:

Thermo Specifications:

Front and back Dial 650, 950
Center Dial 760

1050°C, Nitrogen (10% at 20 psi) bubbling in deionized water.
1 hour oxidation, 0.5 μm thick oxide.

Optional:

Apply hexamethyldisilazane (HMDS).
Adhesion promoter.

Coating:

HPR 504 positive resist (Olin Hunt Speciality Products Inc. - 841233)
Dispense 2-3 ml using a syringe and a #20 needle.
Solitec Spinner Parameters:

Acceleration 700
Spread 400 rpm 3 sec
Spin 3500 rpm 15 sec

Photoresist thickness ~ 1.4 μm.

Soft bake:

To remove all solvents from the resist coating rendering the photoresist photosensitive.
Solitec hot plate parameters:

Temperature 110°C
Vacuum Bake 50 sec
Nitrogen Backfill 10 sec

Expose:

Ultraviolet radiation impinging on the photoresist causes a chemical change in the photoresist.
Quintel Mask Aligner specifications:

Lamp Power 200 W
Exposure 11 sec

Develop:

Microposit developer 354 (Shipley product - LH 010)

Exposed positive photoresist is removed using the developer.

Solitec Spinner Parameters:

PreWet	400 rpm	5 sec
Develop	400 rpm	50 sec
Rinse	400 rpm	90 sec
Spin	3500 rpm	15 sec

Inspection:

Linewidth, Defect count and Alignment.

Hard bake:

Hardens the photoresist to withstand subsequent etching.

Solitec Hot plate Parameters:

Temperature	120°C
Vacuum Bake	60 sec
Nitrogen Backfill	10 sec

Etching:

Buffered Oxide Etchant 10:1 (Phillip A. Hunt chemical corporation - 880061)

(Ammonia fluoride-40%, 10 volumes and Hydrofluoric acid-49%, 1 volume)

Typical etch times for 10:1 BOE:

CVD oxide - 0.1-0.2 μm/min.

Thermal oxide - 0.05 μm/min.

Photoresist strip:

Acetone $(CH_3)_2CO$ (Olin Hunt Speciality Products Inc. - 880022)

Acetone is used to strip the photoresist.

Removes the remaining photoresist and leaves behind the oxide mask.

A.3.2 : ANISOTROPIC ETCHANT FOR SILICON:

Ethylenediamine, Pyracatechol and Water (EDP):

Ethylenediamine, anhydrous (Fisher Scientific - E479-4)

Catechol, pyrocatechin (Fisher Scientific - P370B-500)

Deionized water

Chemical etching specifications :

Ethylenediamine - 750 ml, Pyracatechol - 120 g and water - 240 ml[51].

Temperature ~ 115°C,

Etch Rate <100> ~ 0.8 - 1.0 μm/min

Etch rate ratio <100>/<111> ~ 35:1

Doping dependence ~ > 10^{20} cm^{-3} Boron

Etch rate reduced ~ 20 X

Requires a reflux system, controlled temperature bath, agitation and fume hood.

A.3.3 LOW-PRESSURE CHEMICAL VAPOR DEPOSITION [62-64]:

(i) Equipment details:

Chemical vapor deposition (CVD) is the formation of a stable compound on a heated substrate by the decomposition of gaseous compounds. The important considerations in operating a CVD reactor are uniform temperature profile, proper substrate positioning in the gas flow, and gas flow control. The chemical reaction is carried out under various conditions, such as low temperature, high temperature, atmospheric pressure and low pressure. The low-pressure chemical vapor deposition (LPCVD) process offers several advantages over the conventional CVD system, the most important being better uniformity of the deposited materials over etched steps. Low-temperature processes for depositing phosphorus-doped glass (PSG) and silicon dioxide (SiO_2) are especially popular because these films can be deposited directly over metal films. In addition to its numerous applications in IC devices, such as semiconducting layer, conducting layer, superconducting film, masking layer and passivation layer, CVD is also used for the mass production of optical fibers and low-loss optical waveguides. LPCVD is widely used for the deposition of SiO_2, PSG and Si_3N_4, which are the most commonly used waveguide materials.

Low-pressure chemical vapor deposition is rapidly becoming the dominant CVD technique due to its superior step coverage. Deposition is carried out utilizing the quartz diffusion tube as the reaction chamber with gas pumped into one end and out the other as shown in the Figure A.3.1. The quartz tube is surrounded by a three-zone resistance heater with temperatures in the 300 to 500°C range, as it is a low-temperature oxidation equipment. The quartz tube has a mass flow controller at one end and a vacuum pump on the other end. The substrates are placed perpendicular to the gas flow in a support holder. The main advantage of the horizontal reactor is its ability to process large wafer batches. A drawback is the depletion of the reactant species in the gas as it flows over the wafers, causing the deposition rate to decrease. A flat temperature profile is maintained along the tube, and there are four gas injection ports along the tube to provide uniform deposition rates.

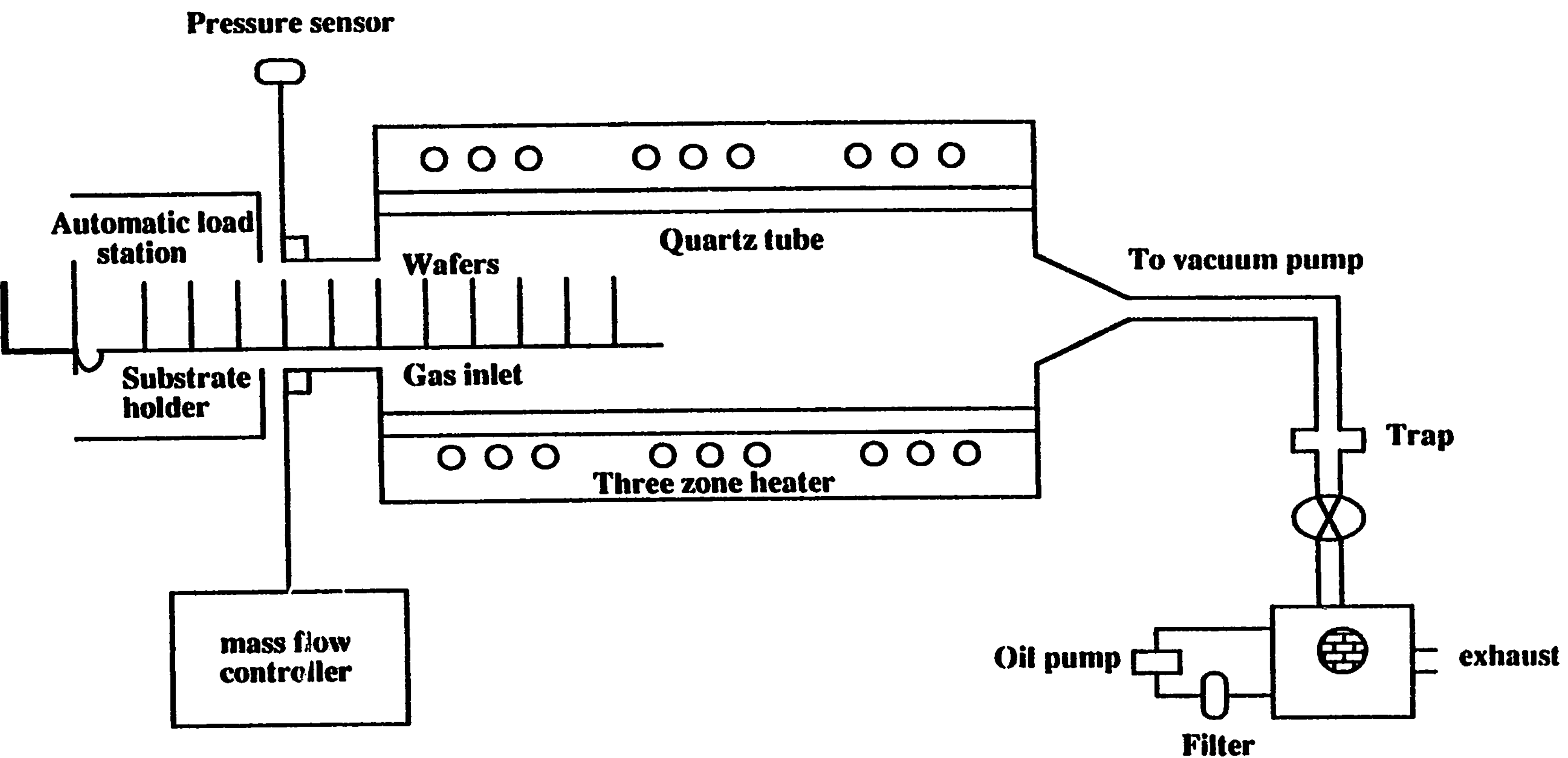

Figure A.3.1 Low-pressure chemical vapor deposition chamber.
(Modified Figure 1.28 from the text Integrated Circuit Fabrication Technology, D.J. Elliot, Mcgraw Hill, 1989).

(ii) CVD Process Theory:

The waveguiding materials used for the optical glass waveguides on silicon were silicon dioxide and phosphorus-doped glass. The waveguides were fabricated at Alberta Microelectronic Centre (AMC) using the LPCVD system, which is also called the LTO (low-temperature oxidation), as it is only used at lower temperatures. The specifications of this LTO system are as follows.

The deposition of low-temperature oxidation results from the surface reaction of silane and oxygen at typical temperatures of 380-450°C for an undoped layer.

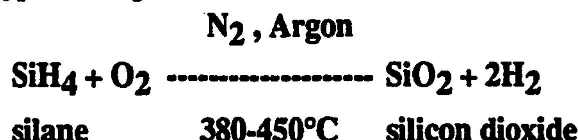

$$\underset{\text{silane}}{SiH_4 + O_2} \xrightarrow[380\text{-}450°C]{N_2\text{, Argon}} \underset{\text{silicon dioxide}}{SiO_2 + 2H_2}$$

The deposition of phosphorus-doped LTO results from the additional surface reaction of phosphine and oxygen at typical temperatures of 380-450°C.

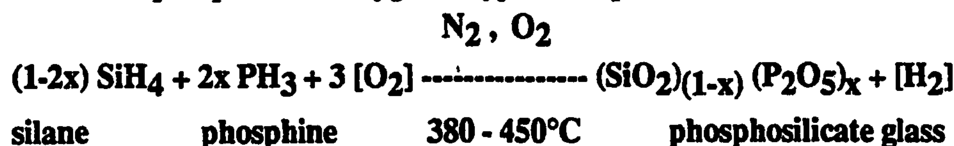

$$\underset{\text{silane}}{(1\text{-}2x)\ SiH_4} + \underset{\text{phosphine}}{2x\ PH_3} + 3\ [O_2] \xrightarrow[380\ -\ 450°C]{N_2\text{, }O_2} \underset{\text{phosphosilicate glass}}{(SiO_2)_{(1\text{-}x)}\ (P_2O_5)_x + [H_2]}$$

The weight percent of phosphorus in the oxide is determined by the flow rate of phosphine during the deposition cycle as a function of the PH_3 / SiH_4 ratio, while the deposition rate of the oxide is controlled by the SiH_4 flow and O_2 / SiH_4 ratio (typically between 2.0 - 2.5). The growth rate is also affected by the deposition temperature and by the addition of phosphine during doped oxide deposition. Deposition rates (angstroms per minute) must be determined for the undoped and doped oxide separately. The deposition rate is also influenced by wafer spacing; increasing the spacing will increase the deposition rate.

(iii) Typical Gas Flows and Temperatures:

Deposition temperature is 430°C.

Deposition pressure is approximately 0.23 Torr.

Deposition rate is approximately 130 Angstrom per minute.

Gas flows during deposition for four inch wafers are as follows:

For silicon dioxide and Phosphorus-doped glass (10 wt.% phosphorus-doped)

Silane (SiH_4) --- 84 sccm

Oxygen (O_2) --- 180 sccm

Phosphine (PH_3) --- 10 sccm (50% of 20 sccm)*

*NOTE: Approximately 1.0 sccm for each weight % (wt. %) phosphine concentration in the oxide using 100% phosphine source.

(iv) Evaluation Methods:

Two critical parameters of the LTO are thickness and phosphorus concentration. Evaluation of thickness is typically with a thin film measurement system. Phosphorus concentration can be determined by wet chemical analysis, flame emission spectroscopy, Auger analysis, microprobe, X-ray techniques and refractive index, as well as etch rate study calibrated to one of the above methods.

A.3.4 DEPOSITION OF VARIOUS METAL FILMS [64]:

Vacuum deposition techniques are used to deposit thin metal films in the semiconductor industry. Thermal evaporation, electron-beam evaporation and sputtering are the most common metal deposition techniques. In the case of evaporation, thin metal films are formed by depositing a material vaporized in a vacuum chamber (at a pressure of less than 10^{-5} Torr) on a substrate. The choice of a heating method depends on the melting temperatures of the materials. In general, the thermal resistance heating method is used for low melting temperature materials, and electron-beam heating or sputtering is used for high melting temperature materials. Thermal evaporation is accomplished by gradually increasing the current flowing through the filament to first melt and then evaporate the material on to the substrate. Electron beam evaporation uses a focused intense beam of electrons to heat and evaporate the material to be deposited. In the sputtering method of vacuum deposition, ions of an inert gas at low-pressure, such as argon, bombards and dislodges atoms from a target of the material to be deposited. The maximum temperature which can be used in processing after metallization is limited by the melting point of the eutectic formed between the silicon and the metallization rather than the melting point of the metal itself [48]. The characterization of the metal films with oxide is as shown in the Figure A.3.2. The reflectivity was measured using the Varian spectrophotometer. The following are the deposited metal films with their surface property and reflectivity details.

SILVER: The thickness of the silver film thermally evaporated on a silicon wafer at 13-15 Å/sec was 1054 Å. The silver film had reflectivity above 98.5% in the wavelength range 600-1550 nm. After the silicon dioxide was deposited, the silver film tarnished and turned hazy. The silver film did not withstand the temperature rise during the CVD process, although its melting point was 962°C. The silver film curled into a blob and its reflectivity was zero. The scanning electron micrograph {Figure A.3.2 (a)} of the surface of the silver film reveals the agglomeration process, formation of spherical caps and beads due to rise in temperature.

CHROME-GOLD: The gold film does not adhere well to silicon or silicon dioxide, so a 200 Å layer of chrome film at 2-3 Å/sec was first thermally evaporated on a silicon wafer and then a 1007 Å thick gold film at 8-9 Å/sec was immediately evaporated. The gold film had a reflectivity of 95% at 633 nm and above 98% at the wavelength range 750-1550 nm. The gold film, which had a melting point of 1064°C developed stress cracks during the silicon dioxide CVD process {see Figure A.3.2 (b)}. This was due to the fact that the Au-Si eutectic temperature was 370°C. The variation of thickness was observed by the size of the hatch marks along the surface, the center ones being larger than than the edge ones. The gold film was no longer pure or reflective.

ALUMINUM: The aluminum film was thermally evaporated, electron beam evaporated and also sputtered. In aluminum metallized surfaces, deposited silicon dioxide and phosphosilicate glass have better adhesion.

Thermal: The thermally-evaporated aluminum is often contaminated, which may be due to the filament or poor handling. The film was 1024 Å thick, deposited at the rate of 11 Å/sec on a silicon wafer. The reflectivity was about 90% at 633 nm, dropped between 700-900 nm and then increased to 95% above 900 nm. The melting point of aluminum is about 660°C. The Al-Si eutectic temperature is 577°C. The deposition of silicon dioxide at 450°C decreased the reflectivity by a very small percentage and resulted in pinhole defects and nodule growth.

Electron-beam: The electron-beam evaporated aluminum is very pure, reflective and is evaporated at higher deposition rates. The 1000 Å thick film with a deposition rate of 25 Å/sec was deposited on a 0.5 μm layer of thermal oxide grown on a silicon wafer. The reflectivity was 91% at 633 nm, dropped between 700-900 nm and then increased to 96%. The aluminum film had excellent reflectivity of 87% after the deposition of silicon dioxide. Also the number of pinholes observed under the optical microscope looked fewer. The SEM pictures {Figure A.3.2 (c)} indicate that very few nodules are formed and there are many small spherical caps on the surface due to the rise in temperature which is a indication of an agglomeration process. The layer of thermal oxide made a difference in the deposition of 2 μm of CVD oxide by isolating silicon and aluminum during the temperature rise which may be the reason for the fewer pinhole defects and smaller and fewer nodules.

Sputter: The sputtered aluminum is an alloy consisting of aluminum and a small percentage of copper which does not give a pure quality film. The film was 1000 Å thick with a reflectivity of 89% at 633 nm, decreasing and then increasing at 900 nm. The layer of CVD oxide reduced the reflectivity to 77% and the film had pinhole defects and

turned hazy. The SEM picture {Figure A.3.2 (d)} reveal that the size of the nodules are very small and there is a indication of an agglomeration process.

COPPER: The copper film was electron-beam-evaporated on a 0.5 μm of thermal oxide grown on a silicon wafer. The layer of thermal oxide was required to prevent the formation of silicides. The copper film was 1019 Å with a deposition rate of 70 Å/sec. It had a reflectivity of 96% at 633 nm and increased to 97% at higher wavelengths. The copper film had a high melting point of 1358°C. The reflectivity decreased to 26% after a layer of CVD oxide was deposited and this may due to the formation of copper oxide. The SEM picture {Figure A.3.2 (e)} reveals that the surface is covered with small spherical caps.

TITANIUM: The titanium film 1000 Å thick was sputtered on a silicon wafer. The film had a reflectivity of 57% at 633 nm and increased to 67% at higher wavelengths. The titanium film had a melting point of 1660°C. The deposition of CVD oxide decreased the reflectivity by a small factor. The SEM picture {Figure A.3.2 (f)} reveals that the surface is covered with small spherical caps. Even after a high temperature anneal at 1050°C the film reflectivity remained the same.

CHROMIUM: The chromium film 1165 Å thick was electron-beam-deposited at the rate of 50 Å/sec on a silicon wafer. The melting point of chromium was 1857°C. The film had a reflectivity of 50-55% at wavelengths above 500 nm. The film turned yellowish-pink in color with a very low reflectivity of 12% after the CVD oxide was deposited. The SEM picture {Figure A.3.2 (g)} reveals that the surface is covered with small spherical caps .

MOLYBDENUM: The molybdenum film 995 Å thick was electron-beam-deposited at the rate of 1 Å/sec on a silicon wafer. The low deposition rate was due to the very high melting point of the molybdenum, which is about 2617°C. The film had a low reflectivity of 39% at 633 nm and 54% at higher wavelengths compared to other metal films. The film turned yellowish-pink in color with a very low reflectivity of 16% after the CVD oxide was deposited. The SEM {Figure A.3.2 (h)} picture reveals that the surface is covered with small spherical caps.

Most of these films have surface defects or low reflectivity which might result in propagation loss due to scattering. The best film for the optical taps would be titanium, which withstands the annealing temperatures.

Figure A.3.2 Characterization of the surface properties of the metal films with oxide.

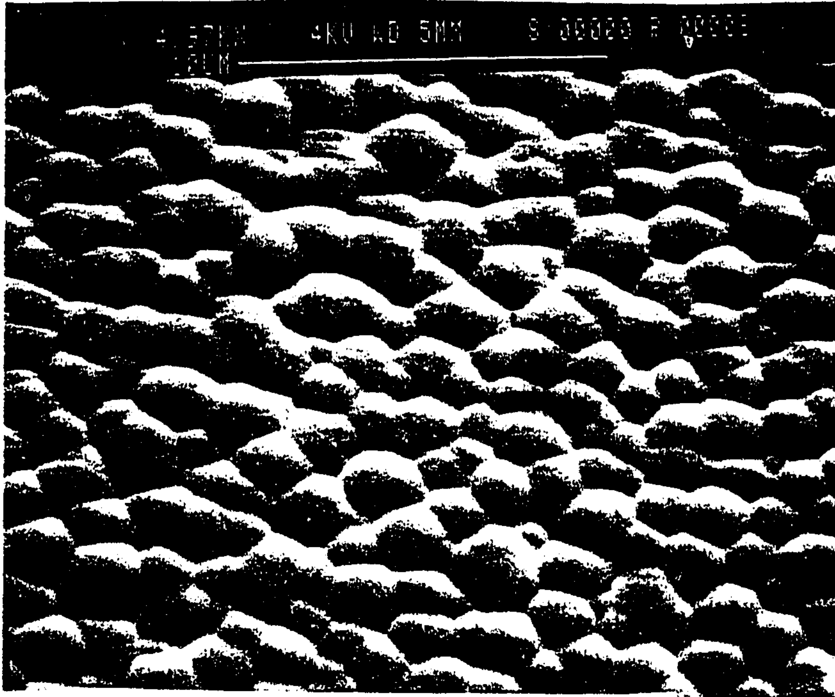

(a) Agglomeration process on silver film with oxide.

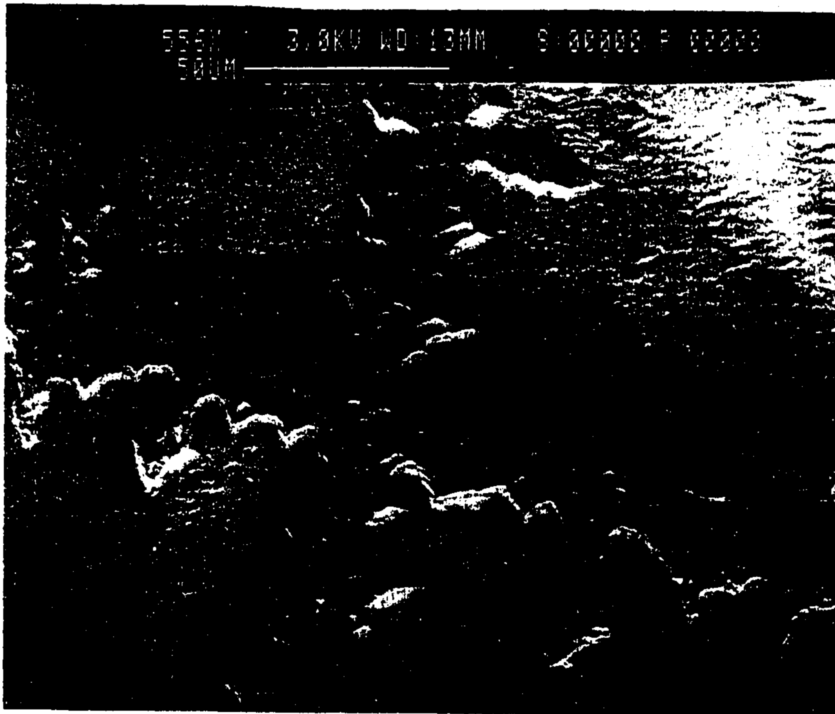

(b) Stress hatch marks on gold film with oxide.

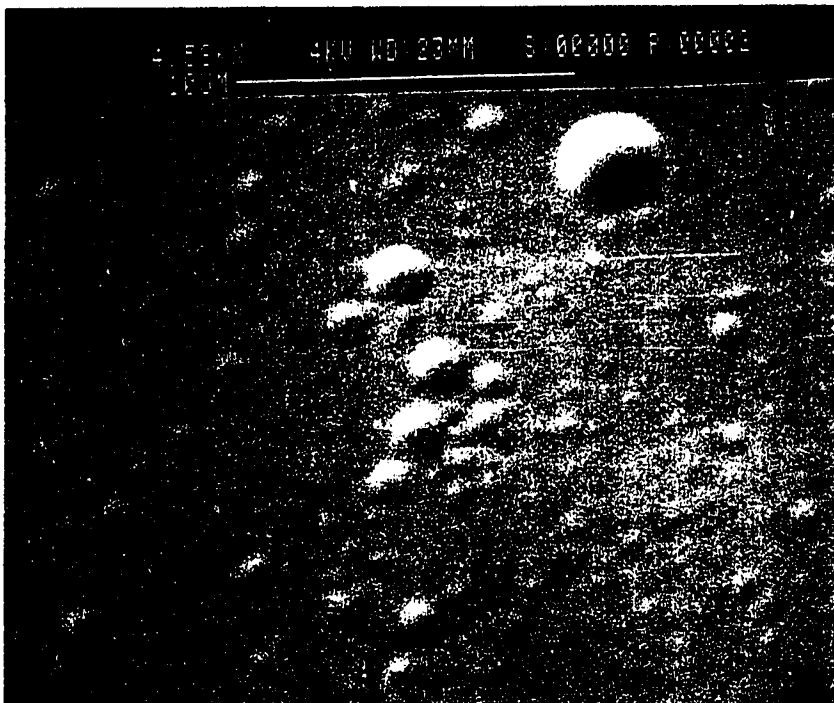

(c) Nodule growth in electron beam evaporated Aluminum film with oxide.

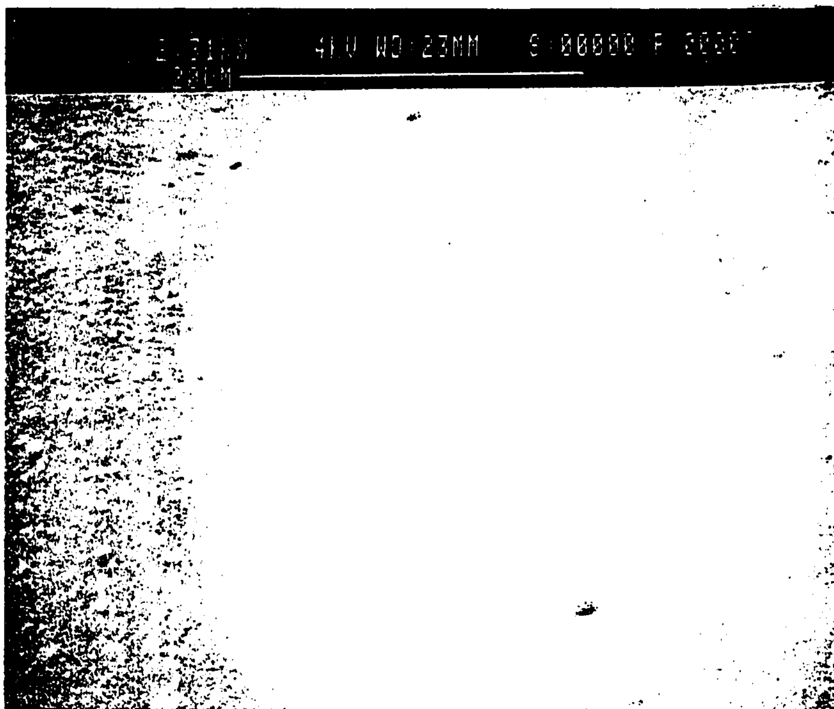

(d) Pinholes and nodules on sputtered aluminum film with oxide.

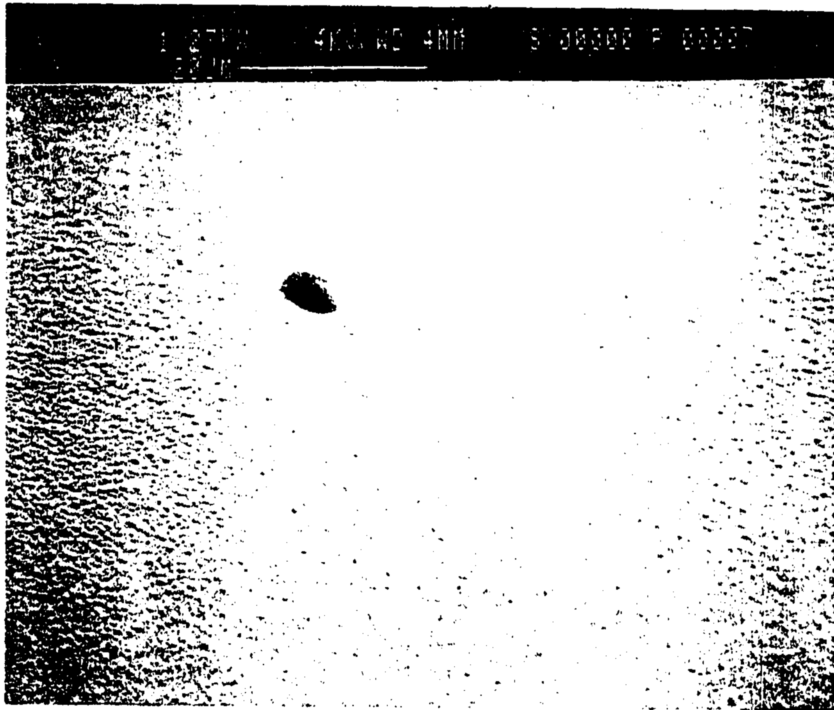

(e) Small spherical caps on copper film with oxide.

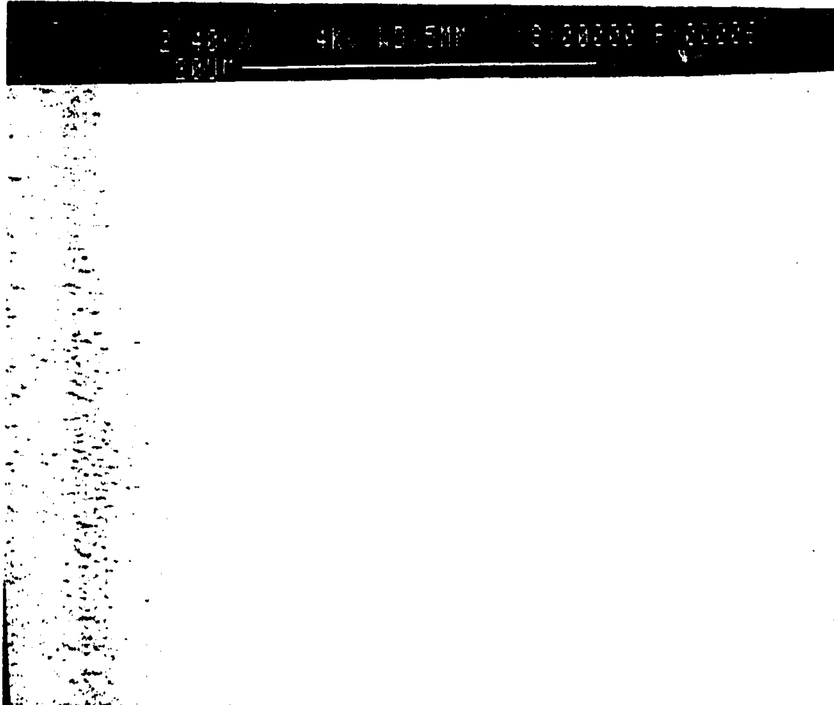

(f) Small spherical caps on titanium film with oxide.

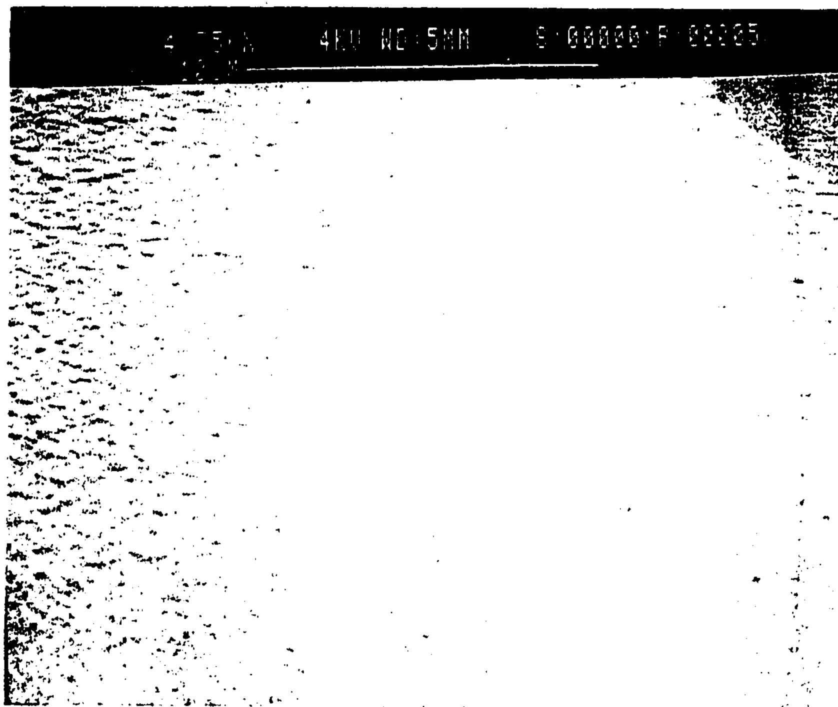

(g) Small spherical caps on chromium film with oxide.

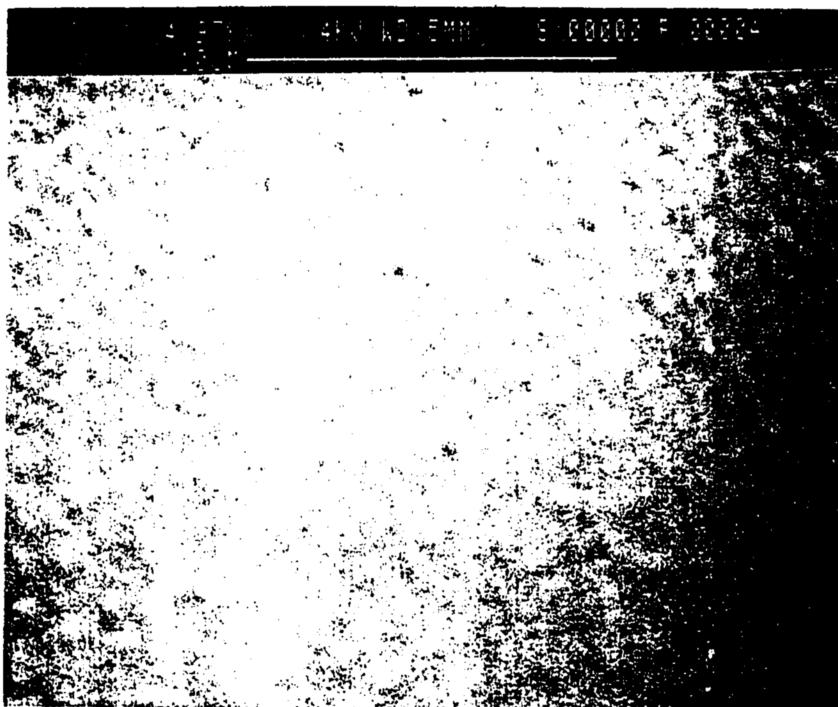

(h) Small spherical caps on molybdenum film with oxide.

APPENDIX 4

Table A.4.1 Loss data of annealed phosphorus-doped glass slab waveguide 1.

SCATTERING LOSS : RELATIVE POWER (dB) VS. DISTANCE (mm)			
DISTANCE (mm)	**POWER (%)**	**POWER (log)**	**POWER (dB)**
1.0	2.750	0.439	4.393
2.0	2.670	0.427	4.265
3.0	2.550	0.407	4.065
4.0	2.314	0.364	3.644
5.0	2.000	0.301	3.010
6.0	1.600	0.204	2.041
7.0	1.575	0.197	1.973
8.0	1.450	0.161	1.614
9.0	1.250	0.097	0.969
10.0	1.350	0.130	1.303
11.0	1.250	0.097	0.969
12.0	1.340	0.127	1.271
13.0	1.225	0.088	0.881
14.0	1.100	0.041	0.414
15.0	1.100	0.041	0.414
16.0	1.220	0.086	0.864
17.0	1.175	0.070	0.700
18.0	1.125	0.051	0.512
19.0	0.950	-0.022	-0.223
20.0	0.825	-0.084	-0.835
21.0	0.800	-0.097	-0.969

Table A.4.2 Loss data of annealed phosphorus-doped glass slab waveguide 2.

SCATTERING LOSS : RELATIVE POWER (dB) VS. DISTANCE (mm)			
DISTANCE (mm)	**POWER (%)**	**POWER (log)**	**POWER (dB)**
1.0	6.000	0.778	7.782
2.0	5.500	0.740	7.404
3.0	5.000	0.699	6.990
4.0	4.500	0.653	6.532
5.0	4.000	0.602	6.021
6.0	3.900	0.591	5.911
7.0	3.650	0.562	5.623
8.0	3.466	0.540	5.398
9.0	3.260	0.513	5.132
10.0	3.220	0.508	5.079
11.0	3.060	0.486	4.857
12.0	2.900	0.462	4.624
13.0	2.875	0.459	4.586
14.0	2.663	0.425	4.254
15.0	2.750	0.439	4.393
16.0	2.550	0.407	4.065
17.0	2.200	0.342	3.424
18.0	2.000	0.301	3.010
19.0	1.800	0.255	2.553
20.0	1.650	0.217	2.175
21.0	1.500	0.176	1.761

Table A.4.3 Loss data of unannealed phosphorus-doped glass slab waveguide 1.

SCATTERING LOSS : RELATIVE POWER (dB) VS. DISTANCE (mm)			
DISTANCE (mm)	**POWER (%)**	**POWER (log)**	**POWER (dB)**
1.0	16.850	1.227	12.266
2.0	16.825	1.226	12.260
3.0	16.800	1.225	12.253
4.0	16.790	1.225	12.251
5.0	16.730	1.223	12.235
6.0	16.730	1.223	12.235
7.0	16.680	1.222	12.222
8.0	16.630	1.221	12.209
9.0	16.590	1.220	12.198
10.0	16.630	1.221	12.209
11.0	16.590	1.220	12.198
12.0	16.530	1.218	12.183
13.0	16.560	1.219	12.191
14.0	16.610	1.220	12.204
15.0	16.550	1.219	12.188
16.0	16.570	1.219	12.193
17.0	16.600	1.220	12.201
18.0	16.580	1.220	12.196
19.0	16.460	1.216	12.164
20.0	16.600	1.220	12.201
21.0	16.440	1.216	12.159
22.0	16.430	1.216	12.156
23.0	16.450	1.216	12.162
24.0	16.320	1.213	12.127
25.0	16.400	1.215	12.148
26.0	16.270	1.211	12.114
27.0	16.260	1.211	12.111

Table A.4.4 Loss data of unannealed phosphorus-doped glass slab waveguide 2.

SCATTERING LOSS : RELATIVE POWER (dB) VS. DISTANCE (mm)			
DISTANCE (mm)	POWER (%)	POWER (log)	POWER (dB)
1.0	50.460	1.703	17.029
2.0	50.180	1.701	17.005
3.0	50.080	1.700	16.997
4.0	49.940	1.698	16.984
5.0	49.850	1.698	16.977
6.0	49.840	1.698	16.976
7.0	49.570	1.695	16.952
8.0	50.008	1.699	16.990
9.0	49.450	1.694	16.942
10.0	48.820	1.689	16.886
11.0	49.750	1.697	16.968
12.0	48.590	1.687	16.865
13.0	48.370	1.685	16.846
14.0	49.360	1.693	16.934
15.0	48.340	1.684	16.843
16.0	48.430	1.685	16.851
17.0	49.200	1.692	16.920
18.0	48.090	1.682	16.821
19.0	49.130	1.691	16.913
20.0	48.590	1.687	16.865
21.0	48.450	1.685	16.853
22.0	48.360	1.684	16.845
23.0	48.880	1.689	16.891
24.0	48.430	1.685	16.851
25.0	48.360	1.684	16.845
26.0	48.340	1.684	16.843
27.0	48.090	1.682	16.821

Table A.4.5 Loss data of phosphorus-doped glass channel waveguide 1.

SCATTERING LOSS : RELATIVE POWER (dB) VS. DISTANCE (mm)			
DISTANCE (mm)	POWER (%)	POWER (log)	POWER (dB)
1.0	8.930	0.951	9.509
2.0	5.960	0.775	7.752
2.5	4.020	0.604	6.042
3.0	3.880	0.589	5.888
3.5	3.430	0.535	5.353
4.0	2.920	0.465	4.654
5.0	1.970	0.294	2.945
6.0	1.870	0.272	2.718
7.0	1.900	0.279	2.788
8.0	1.950	0.290	2.900
9.0	1.560	0.193	1.931
10.0	1.200	0.079	0.792
12.0	1.240	0.093	0.934
14.0	1.300	0.114	1.139
16.0	1.070	0.029	0.294
18.0	0.980	-0.009	-0.088
20.0	0.860	-0.066	-0.655
22.0	0.950	-0.022	-0.223
24.0	0.830	-0.081	-0.809
26.0	0.950	-0.022	-0.223
28.0	0.850	-0.071	-0.706
30.0	0.880	-0.056	-0.555
32.0	0.800	-0.097	-0.969
34.0	0.930	-0.032	-0.315
36.0	0.980	-0.009	-0.088
38.0	0.860	-0.066	-0.655
40.0	0.830	-0.081	-0.809
42.0	0.830	-0.081	-0.809
44.0	0.770	-0.114	-1.135
46.0	0.930	-0.032	-0.315
48.0	0.860	-0.066	-0.655
50.0	0.840	-0.076	-0.757
52.0	0.875	-0.058	-0.580
54.0	0.940	-0.027	-0.269
56.0	0.860	-0.066	-0.655
58.0	0.960	-0.018	-0.177
60.0	0.750	-0.125	-1.249

Table A.4.6 Loss data of phosphorus-doped glass channel waveguide 2.

SCATTERING LOSS : RELATIVE POWER (dB) VS. DISTANCE (mm)			
DISTANCE (mm)	POWER (%)	POWER (log)	POWER (dB)
1.0	10.340	1.015	10.145
2.0	7.330	0.865	8.651
2.5	6.280	0.798	7.980
3.0	5.280	0.723	7.226
3.5	4.480	0.651	6.513
4.0	3.460	0.539	5.391
4.5	3.730	0.572	5.717
5.0	3.030	0.481	4.814
6.0	2.400	0.380	3.802
7.0	2.880	0.459	4.594
8.0	2.940	0.468	4.683
9.0	2.340	0.369	3.692
10.0	2.050	0.312	3.118
11.0	1.780	0.250	2.504
12.0	1.140	0.057	0.569
13.0	0.960	-0.018	-0.177
14.0	0.988	-0.005	-0.052
15.0	0.930	-0.032	-0.315
16.0	0.980	-0.009	-0.088
17.0	0.960	-0.018	-0.177
18.0	0.963	-0.016	-0.164
19.0	0.950	-0.022	-0.223
20.0	0.980	-0.009	-0.088
22.0	0.800	-0.097	-0.969
24.0	0.943	-0.025	-0.255
26.0	0.875	-0.058	-0.580
28.0	0.850	-0.071	-0.706
30.0	0.873	-0.059	-0.590
32.0	0.743	-0.129	-1.290
34.0	1.000	0.000	0.000
36.0	0.871	-0.060	-0.600
38.0	0.914	-0.039	-0.391
40.0	0.943	-0.025	-0.255
42.0	0.890	-0.051	-0.506
44.0	0.950	-0.022	-0.223
46.0	0.900	-0.046	-0.458
48.0	0.750	-0.125	-1.249
50.0	0.830	-0.081	-0.809
52.0	0.800	-0.097	-0.969
54.0	0.850	-0.071	-0.706
56.0	0.760	-0.119	-1.192
58.0	0.810	-0.092	-0.915
60.0	0.750	-0.125	-1.249

Table A.4.7 Horizontal scan data of the output mode profile.

HORIZONTAL SCAN DATA OF MODE PROFILE:		
DISTANCE (PXL)	DISTANCE (um)	INTENSITY
1.0	0.132	66.0
2.0	0.264	64.0
3.0	0.396	62.0
4.0	0.528	63.0
5.0	0.660	63.0
6.0	0.792	66.0
7.0	0.924	69.0
8.0	1.056	75.0
9.0	1.188	71.0
10.0	1.320	75.0
11.0	1.452	74.0
12.0	1.584	82.0
13.0	1.716	97.0
14.0	1.848	92.0
15.0	1.980	105.0
16.0	2.112	112.0
17.0	2.244	124.0
18.0	2.376	131.0
19.0	2.508	135.0
20.0	2.640	144.0
21.0	2.772	150.0
22.0	2.904	160.0
23.0	3.036	160.0
24.0	3.168	167.0
25.0	3.300	176.0
26.0	3.432	180.0
27.0	3.564	181.0
28.0	3.696	185.0
29.0	3.828	193.0
30.0	3.960	196.0
31.0	4.092	195.0
32.0	4.224	196.0
33.0	4.356	192.0
34.0	4.488	195.0
35.0	4.620	195.0
36.0	4.752	189.0
37.0	4.884	190.0
38.0	5.016	185.0
39.0	5.148	185.0
40.0	5.280	179.0
41.0	5.412	166.0
42.0	5.544	172.0
43.0	5.676	164.0

DISTANCE (PXL)	DISTANCE (um)	INTENSITY
44.0	5.808	162.0
45.0	5.940	149.0
46.0	6.072	140.0
47.0	6.204	140.0
48.0	6.336	134.0
49.0	6.468	129.0
50.0	6.600	121.0
51.0	6.732	113.0
52.0	6.864	107.0
53.0	6.996	102.0
54.0	7.128	92.0
55.0	7.260	92.0
56.0	7.392	86.0
57.0	7.524	78.0
58.0	7.656	74.0
59.0	7.788	70.0
60.0	7.920	68.0
61.0	8.052	67.0
62.0	8.184	65.0
63.0	8.316	64.0
64.0	8.448	58.0
65.0	8.580	65.0

Table A.4.8 Vertical scan data of the output mode profile.

VERTICAL SCAN DATA OF MODE PROFILE:		
DISTANCE (PXL)	DISTANCE (um)	INTENSITY
1.0	0.132	58.0
2.0	0.264	58.0
3.0	0.396	54.0
4.0	0.528	63.0
5.0	0.660	61.0
6.0	0.792	49.0
7.0	0.924	59.0
8.0	1.056	62.0
9.0	1.188	60.0
10.0	1.320	66.0
11.0	1.452	65.0
12.0	1.584	68.0
13.0	1.716	75.0
14.0	1.848	74.0
15.0	1.980	75.0
16.0	2.112	85.0
17.0	2.244	91.0
18.0	2.376	93.0
19.0	2.508	108.0
20.0	2.640	113.0
21.0	2.772	121.0
22.0	2.904	122.0
23.0	3.036	137.0
24.0	3.168	137.0
25.0	3.300	145.0
26.0	3.432	152.0
27.0	3.564	164.0
28.0	3.696	166.0
29.0	3.828	168.0
30.0	3.960	170.0
31.0	4.092	179.0
32.0	4.224	180.0
33.0	4.356	185.0
34.0	4.488	186.0
35.0	4.620	194.0
36.0	4.752	191.0
37.0	4.884	194.0
38.0	5.016	195.0
39.0	5.148	194.0
40.0	5.280	192.0
41.0	5.412	191.0
42.0	5.544	191.0
43.0	5.676	187.0

DISTANCE (PXL)	DISTANCE (um)	INTENSITY
44.0	5.808	183.0
45.0	5.940	184.0
46.0	6.072	176.0
47.0	6.204	170.0
48.0	6.336	168.0
49.0	6.468	161.0
50.0	6.600	156.0
51.0	6.732	147.0
52.0	6.864	136.0
53.0	6.996	139.0
54.0	7.128	123.0
55.0	7.260	112.0
56.0	7.392	114.0
57.0	7.524	101.0
58.0	7.656	79.0
59.0	7.788	91.0
60.0	7.920	84.0
61.0	8.052	70.0
62.0	8.184	71.0
63.0	8.316	61.0
64.0	8.448	67.0
65.0	8.580	62.0
66.0	8.712	43.0
67.0	8.844	55.0
68.0	8.976	56.0
69.0	9.108	53.0
70.0	9.240	51.0
71.0	9.372	49.0